Nuclear Physics **A516** (1990) 513-548
North-Holland

MESON EXCHANGE MODEL FOR PSEUDOSCALAR MESON–MESON SCATTERING*

D. LOHSE, J.W. DURSO[1], K. HOLINDE and J. SPETH[2]

Institut für Kernphysik, Kernforschungsanlage Jülich, D-5170 Jülich, Fed. Rep. Germany

Received 2 November 1989
(Revised 23 April 1990)

Abstract: A dynamical model for pseudoscalar–pseudoscalar meson scattering based on meson exchange, suitable for use in a variety of low- and intermediate-energy mesonic interactions, has been constructed and applied to $\pi\pi$ and $K\pi$ scattering with good quantitative results. The model includes both s- and t-channel exchange, and is found to require pseudoscalar–pseudoscalar coupling to a scalar octet to fit the high energy s-wave phases in the $I=0$ $\pi\pi$ channel and in the $I=\frac{1}{2}$ $K\pi$ channel. Coupling of the $\pi\pi$ and $K\bar{K}$ channels is found to play a crucial role in explaining the S*(975) resonance.

1. Introduction

It is generally accepted that quantum chromodynamics (QCD) is the fundamental theory of strong interactions. Therefore, in principle, the hadron–hadron interaction is determined by quark–gluon dynamics. Unfortunately, little is known about QCD solutions in the low-energy (non-perturbative) regime, where most of the nuclear and medium energy physics experiments take place. In this region, however, there are indications [1]) that most of the dynamics can be understood in terms of color-neutral objects, i.e. nucleons, mesons and isobars. Therefore, in the low-energy region (low compared to the perturbative QCD-regime), the strong interaction can probably be described to a very good approximation within the framework of meson-exchange interactions. The basic ingredients of such models are meson–baryon–baryon and meson–meson–meson vertices which represent an effective description of the very complicated, and mathematically yet intractable, multi-quark and gluon exchanges. These vertices contain coupling constants and form factors which parametrize the finite size of the hadrons. It is obvious that the meson-exchange model is limited in its applicability, and that one expects corrections due to the underlying quark structure. The interesting question, however, is where do we see those "quark effects" in nuclear and medium energy physics? Alternatively one may ask: to what extent can nuclear and intermediate-energy physics be described by conventional meson and baryon exchange without reference to the quark degrees

* Supported in part NATO grant TG.85/0093.

[1] On leave from Mount Holyoke College, South Hadley, MA 01075, USA.

[2] Also at Institut für Theoretische Kernphysik, Universität Bonn, D-5300 Bonn, Fed. Rep. Germany.

of freedom? As the radii of hadrons are given not only by the size of the confining region of the quarks, but also by the extension of the surrounding meson cloud, the range of applicability of the meson-exchange models may be much larger than one expects from oversimplified estimates based on the hadron size.

The development of the Bonn NN potential [2]), which is based on suitably chosen non-strange meson-baryon-baryon vertices, is addressed to the latter question. It, and subsequent extensions [3,4]) to include strange particles, have resulted in a good quantitative description of NN, NΛ, NΣ, and K$^+$N scattering with a consistent set of coupling constants and form factors. The principal aim of this work is to extend the framework of the previous work to include meson-meson interactions: that is, to investigate how well and how high in energy the interaction between mesons can likewise be described by the exchange of known mesons. Thus we model the strong interaction between those mesons and, as the next step, fit the $\pi\pi$ and Kπ data with the model. It is hoped that ultimately a single, consistent set of vertex parameters will yield a good quantitative description of all baryon-baryon, meson-baryon, and meson-meson data up to energies on the order of 1 GeV.

We wish to emphasize at this point that, although we fix the parameters of the model we construct by requiring it to describe $\pi\pi$ and Kπ data very well, a parametrization of the on-shell meson-meson scattering amplitudes is not our aim. Our ultimate aim is to construct a *dynamical* model of the pseudoscalar-pseudoscalar meson interaction which will be useful in applications which require a reliable off-shell extrapolation of the amplitudes and low and intermediate energies, such as final-state interactions in K-decay [5]) or pion double charge-exchange on nuclei. The fit of the model to the $\pi\pi$ and Kπ amplitudes is, then, more in the nature of a boundary condition than an objective in itself. Our approach is a nuclear physics approach and orthogonal that of S-matrix theory in either its dispersive or dual model expressions. Clearly it is also semi-phenomenological in character. While its ingredients are known mesons, we exploit the freedom in the form factors to compensate for suppressed or missing degrees of freedom. That they *are* of short range and that the quantum numbers of the exchanged mesons appear to be just those needed for a good description of the data offers some hope that our aim is at least partially achievable.

In the systems which have been investigated previously, a repulsive core provided by the exchange of vector mesons, especially by ω-exchange, prevents the two hadrons from coming too close to each other, so that one may argue that quark effects in those cases are not so obvious. In the case of two pseudoscalar mesons that we are investigating here, this repulsive ω-exchange is missing, and therefore quark effects might show up more clearly. Indeed, we will see that in order to understand theoretically the weak interaction at threshold in the spin-parity $(J^\pi) = 0^+$ and isospin $(I) = 0$ channel of the $\pi\pi$ system, and in the $J^\pi = 0^+$, $I = \frac{1}{2}$ channel of the Kπ system, respectively, one has to introduce a repulsive piece of very short range into the interaction that cannot be directly connected with experimentally

known mesons. This repulsion is necessary in order to cancel at threshold the attraction provided by scalar meson exchange. However, we will also demonstrate that this effect depends on the way in which scalar mesons are coupled to the pseudoscalar mesons. If we use scalar coupling one needs the above-mentioned additional repulsion, but if we use derivative coupling this repulsive contribution is no longer necessary.

In this paper we will discuss four major points:

(i) We investigate the strong interaction between two pseudoscalar mesons in the framework of the meson-exchange model.

(ii) We analyse the $\pi\pi$ and $K\pi$ scattering data in a coupled channel approach using this meson-exchange interaction.

(iii) We explain the resonance S*(975) in the $\pi\pi$ system in a natural way as a quasibound state in the coupled $K\bar{K}$ channel.

(iv) We find the masses of the genuine scalar mesons (with and without strangeness) which belong to the scalar meson nonet, and which can be interpreted as one-quark-one-antiquark systems, to be around 1400 and 1450 MeV, respectively.

One of our main conclusions concerns the role of the t-channel interaction between pseudoscalar mesons. It turns out that the coupling of these correlated systems to the genuine resonances is very strong. The scalar-isoscalar channel - that is the δ_0^0 phase shift - below 1 GeV is essentially determined by the coupled $\pi\pi$ and $K\bar{K}$ channels. This means that in the underlying quark model, correlated two-quark-two-antiquark configurations play an important role in the whole energy range (≤ 1.5 GeV) we have investigated here. Therefore theoretical models in the quark picture which are restricted to correlated quark-antiquark pairs may be too simple for the systems we are discussing.

2. The meson–meson interaction model

2.1. THE GENERAL SCHEME

In our model for the meson-meson interaction we follow as closely as possible the scheme which has been used previously to construct the Bonn NN potential [2]) and various extensions [3,4]). A meson-exchange model for $\pi\pi$ scattering was investigated some time ago by Ferchländer and Schütte [6]). Their interaction model was restricted to meson poles and $K\bar{K}$ and $N\bar{N}$ pairs in the s-channel. These authors did not consider meson exchange in the t-channel, and especially they did not treat $\pi\pi$ scattering as a coupled-channels problem. Therefore they had to introduce the S*(975) as a genuine scalar resonance. Mennessier [7]) has used a very similar model to that of ref. [6]) to examine the effect of $\pi\pi$ and $K\bar{K}$ scalar-isoscalar interactions on meson pair production in $\gamma\gamma$ scattering. He included coupling between the $\pi\pi$ and $K\bar{K}$ channels phenomenologically, but also introduced scalar resonances at approximately 1 GeV and 1.3-1.5 GeV as explicit s-channel poles in the interaction.

More recently Donoghue *et al.* [8]) have analysed $\pi\pi$-scattering data in the framework of a nonlinear chiral lagrangian up to the one-loop order. With an appropriate choice of the four free parameters of their model, fair agreement with the data up to 700 MeV is obtained. As the model is restricted to SU(2), the K mesons are not considered, so that the possibly important effects of coupling in the $\pi\pi$ and $K\bar{K}$ channels are absent.

In our approach we start also from a field-theoretic hamiltonian which contains, apart from the kinetic energy terms, interaction terms of the form of meson–meson–meson couplings, where both strange and non-strange mesons are considered. Therefore $\pi\pi$-$K\bar{K}$ coupling arises in a natural way - by t-channel exchange of vector mesons with the sme coupling constants that appear in the $K\pi$ channel. The total hamiltonian is then

$$H = H_0 + W, \tag{2.1}$$

with the free hamiltonian

$$H_0 = \sum_n \omega_n b_n^+ b_n, \tag{2.2}$$

where b_n^+ and b_n are the creation and destruction operators for mesons that obey the usual commutation relations for bosons. The index n denotes all quantum numbers which are necessary to specify the respective meson completely: momentum, spin, isospin and strangeness. The sum in eq. (2.2) runs over all relevant bosons (π, η, K, ρ, ω, K*, η', φ, f_2, ε, κ, δ) and ω_n is (with an exception to be discussed later) the renormalized (physical) relativistic energy of the mesons. Thus, most self-energy effects are automatically included and need not be evaluated explicitly.

The interaction hamiltonian W is of the form:

$$W = \sum_{\alpha\beta\gamma} W^{(1)}_{\alpha\beta\gamma} b_\alpha b_\beta b_\gamma + \sum_{\alpha\beta\gamma} W^{(2)}_{\alpha\beta\gamma} b^+_\alpha b_\beta b_\gamma \sum_{\alpha\beta\gamma} W^{(3)}_{\alpha\beta\gamma}\, b_\alpha b^+_\beta b_\gamma + \sum_{\alpha\beta\gamma} W^{(4)}_{\alpha\beta\gamma} b_\alpha b_\beta b^+_\gamma + \text{h.c.} \tag{2.3}$$

The vertex functions $W^{(i)}_{\alpha\beta\gamma}$ can be derived from suitable interaction lagrangians, namely

$$L_{\text{pps}} = g_{\text{pps}} m_{\text{p}} \phi_{\text{p}}(x) \phi_{\text{p}}(x) \phi_{\text{s}}(x) \qquad \text{(scalar coupling)}$$

or

$$L_{\text{pps}} = \frac{f_{\text{pps}}}{m_{\text{p}}} \partial^\mu \phi_{\text{p}}(x) \partial_\mu \phi_{\text{p}}(x) \phi_s(x) \qquad \text{(derivative coupling)}$$

and

$$L_{\text{ppv}} = g_{\text{ppv}} \phi_{\text{p}}(x) \partial_\mu \phi_{\text{p}}(x) \phi_{\text{v}}^\mu(x),$$

$$L_{\text{ppt}} = g_{\text{ppt}} \frac{2}{m_\pi} \partial_\mu \phi_{\text{p}}(x) \partial_\nu \phi_{\text{p}}(x) \phi_{\text{t}}^{\mu\nu}. \tag{2.4}$$

Here ϕ_s, ϕ_p, ϕ_v^μ, and $\phi_t^{\mu\nu}$ are the field operators for scalar, pseudoscalar, vector, and tensor mesons, respectively. Note that only the space-spin part is given. The additional SU(3) flavor part, when added, leads to the characteristic coupling constant ratios used in the present paper (see sect. 3). Defining L to be the sum of all these lagrangians, W (eq. (2.3)) is determined from $W = -\int L\, d^3x$. The resulting vertex functions are modified by introducing form factors, F, whose explicit form will be specified later. Treating H in time-ordered perturbation theory, the matrix elements of the transition operator $T(z)$ can be represented by a series expansion defined by all diagrams containing an incoming and outgoing two-meson state, $|b_n b_m\rangle \equiv b_n^+ b_m^+ |0\rangle$, with $|0\rangle$ the vacuum state:

$$\begin{aligned}\langle b_{n'} b_{m'}|T(z)|b_n b_m\rangle = {} & \langle b_{n'} b_{m'}|W\frac{1}{z - H_0 + i\varepsilon}\,W|b_n b_m\rangle \\ & + \langle b_{n'} b_{m'}|W\frac{1}{z - H_0 + i\varepsilon}\,W\frac{1}{z - H_0 + i\varepsilon}\,W\frac{1}{z - H_0 + i\varepsilon}\,W|b_n b_m\rangle \\ & + \cdots, \end{aligned} \tag{2.5}$$

where $z = \omega_n + \omega_m$ is the starting energy.

This series can be partially summed by solving a (three-dimensional) integral equation of Lippmann-Schwinger type:

$$\begin{aligned}\langle b_{n'} b_{m'}|T(z)|b_n b_m\rangle = {} & \delta^{(3)}(\boldsymbol{p}_n + \boldsymbol{p}_m - \boldsymbol{p}_{n'} - \boldsymbol{p}_{m'})\langle b_{n'} b_{m'}|V(z)|b_n b_m\rangle \\ & + \sum_{n''m''} \delta^{(3)}(\boldsymbol{p}_{n''} + \boldsymbol{p}_{m''} - \boldsymbol{p}_{n'} - \boldsymbol{p}_{m'})\langle b_{n'} b_{m'}|V(z)|b_{n''} b_{m''}\rangle \\ & \times \frac{1}{z - \omega_{n''} - \omega_{m''} + i\varepsilon}\langle b_{n''} b_{m''}|T(z)|b_n b_m\rangle . \end{aligned} \tag{2.6}$$

The kernel of this integral equation, the quasipotential $\langle b_{n'} b_{m'}|V(z)|b_n b_m\rangle$, consists of the infinite sum of all diagrams which are irreducible with respect to the entrance channel. Diagrams involving at least one intermediate state consisting of the particles in the entrance channel are generated by the scattering equation.

2.2. COUPLED-CHANNEL FORMALISM

In principle, $V(z)$ contains, for a given entrance (and exit) channel - say $\pi\pi$ - processes with an unlimited number of $K\bar{K}$, $\eta\eta$, $\pi\omega$, $\rho\rho$, etc. intermediate states. Since the $K\bar{K}$ channel will turn out to be of extreme importance, we will treat this channel exactly in a coupled-channels framework. The $\eta\eta$ channel, due to weak coupling to the $\pi\pi$ channel and weak $\eta\eta$ interaction, has negligible effects. Treatment of other channels we defer to a future study. Of course, below the $K\bar{K}$ threshold, this coupling occurs only virtually in the $\pi\pi$ system whereas $K\bar{K}$ scattering, because of real transitions to the $\pi\pi$ system, is inelastic for all energies.

We start by defining, in the c.m. system, channel matrix elements of $V(z)$ and $T(z)$, i.e., $\langle \boldsymbol{p}' | V^{i'i}(z) | \boldsymbol{p} \rangle$. Here $i'(i)$ denotes the outgoing (incoming) channel with $i = 1, 2$ denoting, e.g., the $\pi\pi$ and $K\bar{K}$ channels. Using these definitions, eq. (2.6) can be written as (omitting the δ-functions)

$$\langle \boldsymbol{p}' | T^{i'i}(z) | \boldsymbol{p} \rangle = \langle \boldsymbol{p}' | V^{i'i}(z) | \boldsymbol{p} \rangle + \sum_{i''=1,2} \int \mathrm{d}^3 p'' \langle \boldsymbol{p}' | V^{i'i''}(z) | \boldsymbol{p}'' \rangle \frac{1}{z - \omega_{p''}^{(i'')} + i\varepsilon} \langle \boldsymbol{p}'' | T^{i''i}(z) | \boldsymbol{p} \rangle . \quad (2.7)$$

Here, $\omega_{p''}^{(i'')}$ denotes the intermediate energy in channel i'', i.e.

$$\omega_{q''}^{(1)} = 2\omega_{q''}(\pi) , \qquad \omega_{q''}^{(2)} = 2\omega_{q''}(K) . \quad (2.8)$$

$V^{i'i}$ now consists of a reduced, but in principle still infinite, sum of all processes which are irreducible with respect to both the $\pi\pi$ and $K\bar{K}$ channels.

Eq. (2.7) can be written in matrix form:

$$\langle \boldsymbol{p}' | \boldsymbol{T}(z) | \boldsymbol{p} \rangle = \langle \boldsymbol{p}' | \boldsymbol{V}(z) | \boldsymbol{p} \rangle + \int \mathrm{d}^3 p'' \langle \boldsymbol{p}' | V(z) | \boldsymbol{p}'' \rangle G_0(p'', z) \langle \boldsymbol{p}'' | \boldsymbol{T}(z) | \boldsymbol{p} \rangle \quad (2.9)$$

with the definitions

$$G_0(p'', z) = \begin{pmatrix} \dfrac{1}{z - \omega_{p''}^{(1)} + i\varepsilon} & 0 \\ 0 & \dfrac{1}{z - \omega_{p''}^{(2)} + i\varepsilon} \end{pmatrix},$$

$$\boldsymbol{V}(z) = \begin{pmatrix} V^{11}(z) & V^{12}(z) \\ V^{21}(z) & V^{22}(z) \end{pmatrix}, \quad (2.10)$$

and similarly for $\boldsymbol{T}(z)$.

If we suppress the influence of the direct interaction in channel 2 ($K\bar{K} \to K\bar{K}$) on the interaction in channel 1 ($\pi\pi \to \pi\pi$) by setting $V_{(z)}^{(22)}$ equal to zero, eq. (2.7) can be decoupled,

$$\langle \boldsymbol{p}' | T^{11}(z) | \boldsymbol{p} \rangle = \langle \boldsymbol{p}' | \tilde{V}^{11}(z) | \boldsymbol{p} \rangle + \int \mathrm{d}^3 p'' \langle \boldsymbol{p}' | \tilde{V}^{11}(z) | \boldsymbol{p}'' \rangle \frac{1}{z - \omega_{p''}^{(1)} + i\varepsilon} \langle \boldsymbol{p}'' | T^{11}(z) | \boldsymbol{p} \rangle ,$$

$$\langle \boldsymbol{p}' | T^{21}(z) | \boldsymbol{p} \rangle = \langle \boldsymbol{p}' | V^{21}(z) | \boldsymbol{p} \rangle + \int \mathrm{d}^3 p'' \langle \boldsymbol{p}' | V^{21}(z) | \boldsymbol{p}'' \rangle \frac{1}{z - \omega_{p''}^{(1)} + i\varepsilon} \langle \boldsymbol{p}'' | T^{11}(z) | \boldsymbol{p} \rangle , \quad (2.11)$$

with the effective potential

$$\langle \boldsymbol{p}' | \tilde{V}^{11}(z) | \boldsymbol{p} \rangle = \langle \boldsymbol{p}' | V^{11}(z) | \boldsymbol{p} \rangle + \int \mathrm{d}^3 p'' \langle \boldsymbol{p}' | V^{12}(z) | \boldsymbol{p}'' \rangle \frac{1}{z - \omega^{(2)}_{p''} + i\varepsilon} \langle \boldsymbol{p}'' | V^{21}(z) | \boldsymbol{p} \rangle . \quad (2.12)$$

Thus, in this approximation, the coupling effects of the $K\bar{K}$ channel on the $\pi\pi$ channel are given only by box diagrams with $K\bar{K}$ intermediate states. We will investigate the quality of this approximation later.

2.3. DETERMINATION OF THE QUASIPOTENTIAL $V(z)$

Of course, for practical reasons, one has to restrict oneself to those processes in $V^{i'i}(z)$ which are of relatively low order in W. The processes actually taken into account in our model are shown in fig. 1 for the $\pi\pi$, and in fig. 2 for the $K\pi$ cases. We stress already here that both s- and t-channel $\rho(K^*)$ exchange have to be

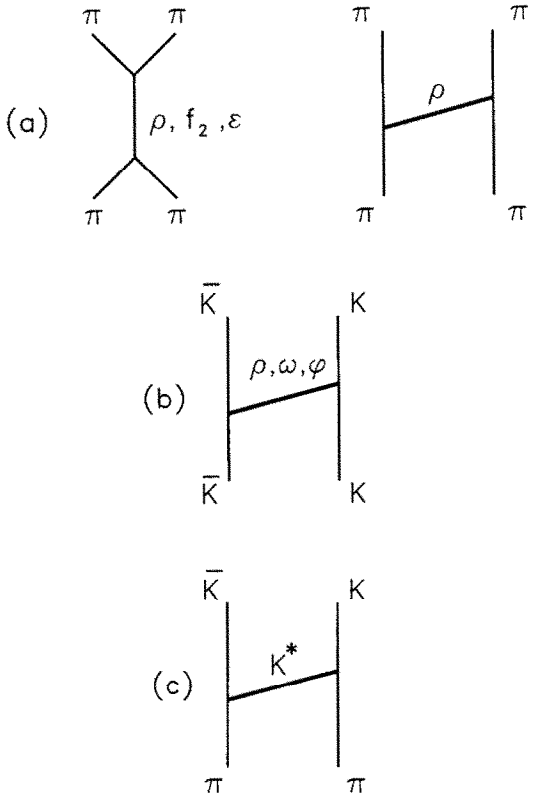

Fig. 1. Diagrams included in our coupled-channel model for the $\pi\pi$ and $\bar{K}K$ interactions, for one of two possible time orderings. (a) contains processes in the $\pi\pi \to \pi\pi$ channel, (b) those in the $\bar{K}K \to K\bar{K}$ channel, and (c) describes the $\pi\pi \to K\bar{K}$ transition.

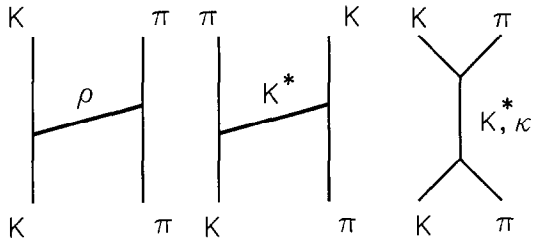

Fig. 2. Diagrams included in our model for the $K\pi$ interaction, for one of two possible time orderings.

considered in the $\pi\pi(K\pi)$ channel in order to achieve a quantitative description of the data. Whereas the scalar-isoscalar $\varepsilon(1400)$, the isoscalar spin-two meson $f_2(1270)$, and the strange $\kappa(1430)$ are definitely needed as s-channel pole graphs to account for the empirically observed resonant behavior in the corresponding partial waves, their t-channel contributions are, because of their large mass, too short-ranged to be of any relevance and are therefore neglected.

Starting from the interaction lagrangians given in eq. (2.4) we obtain for the potential arising from t-channel vector meson exchange, in a general reference frame characterized by incoming (outgoing) four-momenta p_1, p_2 ($p_{1'}$, $p_{2'}$) and corresponding relativistic energies $\omega_i \equiv (\boldsymbol{p}_i^2 + m_i^2)^{1/2}$,

$$\langle 1'2'|V_v^{(t)}(z)|12\rangle = \sum_{\lambda_\alpha} \frac{g_1 g_2}{(2\pi)^3} F^{(t)2}(q_\alpha^2) \frac{n \cdot \mathrm{IF}}{8\omega_\alpha(\omega_{1'}\omega_{2'}\omega_1\omega_2)^{1/2}}$$
$$\times (p_{1'}+p_1)_\mu (p_{2'}+p_2)_\nu \varepsilon^\mu(p_\alpha,\lambda_\alpha)\varepsilon^\nu(p_\alpha,\lambda_\alpha)^*$$
$$\times \left[\frac{1}{z-\omega_{1'}-\omega_2-\omega_\alpha} + \frac{1}{z-\omega_{2'}-\omega_1-\omega_\alpha}\right]. \qquad (2.13)$$

Here, ω_α is the energy of the exchanged vector meson α and $\varepsilon^\mu(p_\alpha,\lambda_\alpha)$ is the polarization vector belonging to a spin-one particle with momentum p_α and helicity λ_α. The factor n is $\frac{1}{2}$ for the $\pi\pi \to \pi\pi$ channel, $\sqrt{\frac{1}{2}}$ for the $\pi\pi \to K\bar{K}$ transition, and 1 for the $K\bar{K} \to K\bar{K}$ channel. IF is a factor depending on the total isospin of the considered reaction; it is given explicitly in table 1 (see the following section). The form factors F will be specified below. Note that eq. (2.13) contains both possible time orderings (see fig. 3a, b).

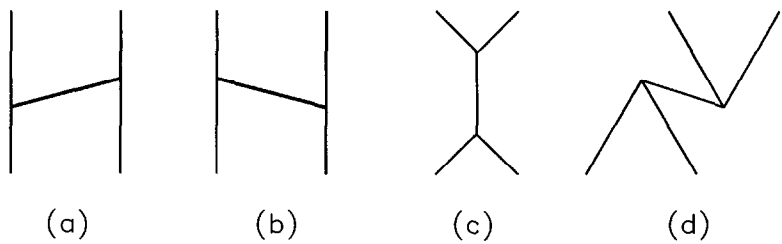

Fig. 3. Time orderings contributing to the t-channel (a, b) and s-channel (c, d) exchange.

The corresponding s-channel process (fig. 3c, d) is described by a similar expression, namely

$$\langle 1'2'|V_{\mathrm{v}}^{(\mathrm{s})}(z)|12\rangle = \sum_{\lambda_\alpha} \frac{g_1 g_2}{(2\pi)^3} F^{(\mathrm{s})^2}(q_\alpha^2) \frac{n\cdot \mathrm{IF}}{8\omega_\alpha(\omega_{1'}\omega_{2'}\omega_1\omega_2)^{1/2}} \times (p_{1'}-p_{2'})_\mu (p_1-p_2)_\nu \varepsilon^\mu(p_\alpha,\lambda_\alpha)\varepsilon^\nu(p_\alpha,\lambda_\alpha)^* \times\left[\frac{1}{z-\omega_\alpha^0}+\frac{1}{z-\omega_{1'}-\omega_{2'}-\omega_1-\omega_2-\omega_\alpha}\right]. \tag{2.14}$$

Here ω_α^0 denotes the energy connected with the bare mass of the particle in the intermediate state which, after unitarization by means of eqs. (2.9)-(2.12), is shifted to the physical mass due to self-energy corrections. In contrast, the t-channel process (eq. (2.13)), as well as the second piece of eq. (2.14) (fig. 3d), should contain the physical mass from the beginning since here unitarization, which occurs in the s-channel only, does not generate corresponding self-energy contributions.

The s-channel processes involving a scalar meson depend on the kind of vertex coupling used. For scalar coupling we have

$$\langle 1'2'|V_{\mathrm{s,S}}^{(\mathrm{s})}(z)|12\rangle = \frac{g_1 g_2}{(2\pi)^3} F^{(\mathrm{s})^2}(q_\alpha^2) \frac{n\cdot \mathrm{IF}}{8\omega_\alpha(\omega_{1'}\omega_{2'}\omega_1\omega_2)^{1/2}} \times m_\pi^2\left[\frac{1}{z-\omega_\alpha^0}+\frac{1}{z-\omega_{1'}-\omega_{2'}-\omega_2-\omega_\alpha}\right] \tag{2.15a}$$

and for gradient coupling

$$\langle 1'2'|V_{\mathrm{s,G}}^{(\mathrm{s})}(z)|12\rangle = \frac{g_1 g_2}{(2\pi)^3} F^{(\mathrm{s})^2}(q_\alpha^2) \frac{n\cdot \mathrm{IF}}{8\omega_\alpha(\omega_{1'}\omega_{2'}\omega_1\omega_2)^{1/2}} \times \frac{(p_{1'}-p_{2'})^2(p_1-p_2)^2}{m_\pi^2}\left[\frac{1}{z-\omega_\alpha^0}+\frac{1}{z-\omega_{1'}-\omega_{2'}-\omega_1-\omega_2-\omega_\alpha}\right].$$

Finally, the tensor meson resonance f_2 results in

$$\langle 1'2'|V_{\mathrm{t}}^{(\mathrm{s})}(z)|12\rangle = \sum_{\lambda_\alpha} \frac{g_1 g_2}{(2\pi)^3} F^{(\mathrm{s})^2}(q_\alpha^2) \frac{n\cdot \mathrm{IF}}{8\omega_\alpha(\omega_{1'}\omega_{2'}\omega_1\omega_2)^{1/2}} \times (p_{1'}-p_{2'})_\mu (p_{1'}-p_{2'})_\nu (p_1-p_2)_\rho (p_1-p_2)_\sigma \varepsilon^{\mu\nu}(p_\alpha,\lambda_\alpha)\varepsilon^{\rho\sigma}(p_\alpha,\lambda_\alpha)^* \times\left[\frac{1}{z-\omega_\alpha^0}+\frac{1}{z-\omega_{1'}-\omega_{2'}-\omega_1-\omega_2-\omega_\alpha}\right], \tag{2.16}$$

with $\varepsilon^{\mu\nu}$ the polarization tensor describing the spin-two meson.

2.4. FORM FACTORS

The potentials contain form factors describing the extended hadron structure. In principle, they are completely determined by the underlying quark-gluon dynamics.

However, because of the enormous complexity of QCD in the low-energy regime, their derivation is not possible at present. Therefore they are suitably parametrized, leading to the required suppression of the meson exchange contributions for higher momentum transfers. Although they depend in general on all three 4-momenta involved at the vertex, they are usually parametrized in a simple form depending only on the 3-momentum of that particle which is exchanged in the corresponding potentials.

For t-channel exchange, we use at each vertex a form factor of conventional monopole type

$$F^{(t)} \equiv F_1(\boldsymbol{q}_\alpha^2) = \frac{\Lambda^2 - m_\alpha^2}{\Lambda^2 + \boldsymbol{q}_\alpha^2}, \tag{2.17}$$

where m_α is the mass of the exchanged meson in the t-channel and $\boldsymbol{q}_\alpha$ its 3-momentum.

When the particle appears as an s-channel resonance we take either the form

$$F^{(s)} \equiv F_2(\omega_p^2) = \frac{\Lambda^2 + m_\alpha^2}{\Lambda^2 + \omega_p^2}, \tag{2.18}$$

where ω_p is the total energy of the incoming (or outgoing) state, or

$$F^{(s)} \equiv F_3(\omega_p^2) = \frac{\Lambda^4 + m^4}{\Lambda^4 + \omega_p^4}. \tag{2.19}$$

The latter form is needed for the gradient coupling of the scalar meson as well as for the tensor meson in order to generate sufficient convergence. The change of the form factor parametrization when going from the t- to the s-channel is necessary and justified since we are in very different kinematic regimes.

2.5. SCATTERING PARAMETERS

In order to obtain the scattering observables we must first perform a partial wave expansion of the quasipotential $V^{i'i}(z)$, namely

$$\langle \boldsymbol{p}' | V^{i'i}(z) | \boldsymbol{p} \rangle = \frac{1}{4\pi} \sum_J (2J+1) P_J(\cos\theta) V_J^{i'i}(p', p|z), \tag{2.20}$$

where θ is the angle between $\boldsymbol{p}$ and $\boldsymbol{p}'$ and

$$V_J^{i'i}(p', p|z) = 2\pi \int_{-1}^{+1} \mathrm{d}\cos\theta \, P_J(\cos\theta) \langle \boldsymbol{p}' | V^{i'i}(z) | \boldsymbol{p} \rangle. \tag{2.21}$$

After an analogous expansion for T, eq. (2.7) for partial waves is

$$T_J^{i'i}(p', p|z) = V_J^{i'i}(p', p|z) + \sum_{i''=1,2} \int_0^\infty \mathrm{d}p'' \, p''^2 V_J^{i'i''}(p', p''|z) \frac{1}{z - \omega_{p''}^{(i'')} + i\varepsilon} T_J^{i''i}(p'', p|z) \tag{2.22}$$

(A corresponding equation is obtained for the uncoupled case, eq. (2.11)). The S-matrix is then obtained from the on-shell T-matrix by

$$S_J^{i'i}(z) = \delta^{i'i} - 2\pi i(\rho^{i'}\rho^{i})^{1/2} T_J^{i'i}(z) \tag{2.23}$$

with density $\rho^i(\rho^{i'})$ in the entrance (exit) channel given by $\rho^i = p^{(i)^2}\, \mathrm{d}p^{(i)}/\mathrm{d}\omega^{(i)}$, $\omega^{(i)}$ being the sum of meson energies in the initial and final channels. These S-matrix elements in channel space are conventionally parametrized by

$$S_J(z) = \begin{pmatrix} \eta_J(z)\, \mathrm{e}^{2i\delta_J^{(1)}(z)} & i\sqrt{1-\eta_J^2(z)}\, \mathrm{e}^{i\delta_J^{(12)}(z)} \\ i\sqrt{1-\eta_J^2(z)}\, \mathrm{e}^{i\delta_J^{(12)}(z)} & \eta_J(z)\, \mathrm{e}^{2i\delta_J^{(2)}(z)} \end{pmatrix}, \tag{2.24}$$

with $\delta_J^{(12)} = \delta_J^{(1)} + \delta_J^{(2)}$.

2.6. NUMERICAL METHODS

Solution of the resulting partial wave equations, for both the coupled and uncoupled channels, is done by straightforward numerical matrix inversion. We use the method of Haftel and Tabakin [9]), generalized to include coupled channels, to regularize the principal value integrals. A 30-point gaussian quadrature yields stable results throughout the energy range considered in this work.

3. Model parameters

3.1. COUPLING CONSTANTS AND SYMMETRIES

For the pseudoscalar-pseudoscalar-vector coupling we determine the coupling constants from the SU(3)-symmetric lagrangian

$$L_{\mathrm{ppv}} = -\tfrac{1}{2} i G_{\mathrm{v}}\, \mathrm{Tr}\,([P, \partial_\mu P]_- V^\mu)\,, \tag{3.1}$$

where P is the 3×3 matrix representation of the pseudoscalar meson octet, $P = \lambda^a P^a$, $a = 1, \ldots, 8$, and λ^a are the 3×3 generators of SU(3). An equivalent definition is used for V^μ. In terms of explicit SU(3) indices, this leads to

$$L_{\mathrm{ppv}} = G_{\mathrm{v}} f^{abc} P^a \partial_\mu P^b V^{c\mu}\,, \tag{3.2}$$

where f^{abc} are the antisymmetric structure constants [10]). This gives the following relations between the relevant pseudoscalar-pseudoscalar-vector coupling constants:

$$\begin{aligned} g_{\pi\pi\rho} &= 2G_{\mathrm{v}}\,, \\ g_{\mathrm{K}\mathrm{K}\rho} &= g_{\overline{\mathrm{K}}\mathrm{K}\rho} = G_{\mathrm{v}}\,, \\ g_{\mathrm{K}\mathrm{K}\omega_8} &= -g_{\overline{\mathrm{K}}\mathrm{K}\omega_8} = \sqrt{3}G_{\mathrm{v}}\,, \\ g_{\mathrm{K}\eta\mathrm{K}^*} &= -g_{\overline{\mathrm{K}}\eta\mathrm{K}^*} = -\sqrt{3}G_{\mathrm{v}}\,, \\ g_{\overline{\mathrm{K}}\pi\overline{\mathrm{K}}^*} &= g_{\mathrm{K}\pi\overline{\mathrm{K}}^*} = -G_{\mathrm{v}}\,, \end{aligned} \tag{3.3}$$

with all others zero. The notation $g_{\alpha\beta\gamma}$ denotes the coupling constant for the process $\alpha+\beta\to\gamma$, and standard isospin-invariant couplings within an isotopic multiplet are implied. Thus, for example, $L_{\pi\pi\rho}=g_{\pi\pi\rho}\varepsilon^{ijk}\pi_i\partial_\mu\pi_j\rho_k^\mu$, and $g_{\mathrm{KK}\rho}=g_{\overline{\mathrm{KK}}\rho}$ implies $g_{\mathrm{K}^+\mathrm{K}^+\rho^0}=g_{\bar{\mathrm{K}}^0\bar{\mathrm{K}}^0\rho^0}=-g_{\mathrm{K}^0\mathrm{K}^0\rho^0}=-g_{\mathrm{K}^-\mathrm{K}^-\rho^0}$. Vector octet-singlet mixing is included, with the mixing angle taken to be "ideal", so that the physical ω-meson contains only non-strange quark-antiquark pairs, and the physical φ-meson is pure $s\bar{s}$. The coupling $g_{\mathrm{KK}\varphi}$ is determined from the empirical width of the φ within the Lee model, which gives $g_{\mathrm{KK}\varphi}\approx\sqrt{\frac{1}{2}}g_{\pi\pi\rho}$ to an accuracy of 1%. In the actual calculation this relation is assumed to hold exactly.

The pseudoscalar-pseudoscalar-scalar coupling to the 0^+ octet and to the 0^+ singlet would, in principle, be given by the SU(3)-symmetric lagrangian

$$L_{\mathrm{pps}}=\tfrac{1}{2}G_{\mathrm{s}}^8\,\mathrm{Tr}\,[P,P]_+S)+\tfrac{1}{2}G_{\mathrm{s}}^1\,\mathrm{Tr}\,([P,P]_+)\varepsilon_1\,, \tag{3.4}$$

where now S is the 3×3 representation of the scalar octet and ε_1 is the scalar SU(3) singlet. In terms of SU(3) indices this gives

$$L_{\mathrm{pps}}=G_{\mathrm{s}}^8 d^{abc}P^aP^bS^c+G_{\mathrm{s}}^1\delta^{ab}P^aP^b\varepsilon_1\,, \tag{3.5}$$

leading to the following relations among the coupling constants:

$$\begin{aligned}
&m_{\mathrm{P}}g_{\pi\pi\varepsilon_8}=2\sqrt{\tfrac{1}{3}}G_{\mathrm{s}}^8\,,\\
&m_{\mathrm{P}}g_{\mathrm{KK}\varepsilon_8}=m_{\mathrm{P}}g_{\overline{\mathrm{KK}}\varepsilon_8}=-\sqrt{\tfrac{1}{3}}G_{\mathrm{s}}^8\,,\\
&m_{\mathrm{P}}g_{\eta\eta\varepsilon_8}=-2\sqrt{\tfrac{1}{3}}G_{\mathrm{s}}^8\,,\\
&m_{\mathrm{P}}g_{\pi\mathrm{K}\kappa}=-m_{\mathrm{P}}g_{\bar{\mathrm{K}}\pi\bar{\kappa}}=G_{\mathrm{s}}^8\,,\\
&m_{\mathrm{P}}g_{\mathrm{K}\eta\kappa}=g_{\bar{\mathrm{K}}\eta\bar{\kappa}}=-\sqrt{\tfrac{1}{3}}G_{\mathrm{s}}^8\,,\\
&m_{\mathrm{P}}g_{\pi\eta\delta}=2\sqrt{\tfrac{1}{3}}G_{\mathrm{s}}^8\,,\\
&m_{\mathrm{P}}g_{\mathrm{KK}\delta}=-m_{\mathrm{P}}g_{\overline{\mathrm{KK}}\delta}=G_{\mathrm{s}}^8\,,
\end{aligned}$$

where δ is the $I=1, S=0$ member of the 0^+ octet, ε_8 is the $I=0$, $S=0$ member, and κ and $\bar{\kappa}$ are the scalar analogs of K and $\bar{\mathrm{K}}$, respectively. For the singlet scalar, the coupling constants are

$$m_{\mathrm{P}}g_{\pi\pi\varepsilon_1}=m_{\mathrm{P}}g_{\mathrm{KK}\varepsilon_1}=m_{\mathrm{P}}g_{\overline{\mathrm{KK}}\varepsilon_1}=m_{\mathrm{P}}g_{\eta\eta\varepsilon_1}=G_{\mathrm{s}}^1\,. \tag{3.7}$$

The lagrangian for derivative coupling to the scalar octet and singlet is taken to be

$$L_{\mathrm{pps}}=\tfrac{1}{2}F_{\mathrm{s}}^8\;\mathrm{Tr}\,[(\partial^\mu P,\partial_\mu P]_+S)+\tfrac{1}{2}F_{\mathrm{s}}^1\,\mathrm{Tr}\,([\partial^\mu P,\partial_\mu P]_+]\varepsilon_1 \tag{3.8}$$

with relations analogous to eq. (3.6) between the coupling constants $f_{\alpha\beta\gamma}^8/m_{\mathrm{P}}$ and F_{s}^8 and $f_{\alpha\beta\gamma}^1/m_{\mathrm{P}}$ and F_{s}^1.

In the limit of exact SU(3) symmetry, m_{P} is the (degenerate) mass of the pseudoscalar octet. Taking $m_{\mathrm{P}}=m_\pi$ everywhere, as is done in this calculation, breaks the SU(3) symmetry of the vertex functions $W_{\alpha\beta\gamma}^{(i)}$.

At the level of the lagrangian, the model is fully crossing-symmetric and, except for mass differences, SU(3)-symmetric as well. Of course, our use of s- and t-channel

form factors, and the unitarization prescription, will violate crossing symmetry, but the same can be said of any unitarization scheme which effectively iterates a subset of diagrams. Thus we must allow the phase shifts, which presumably reflect all the symmetries, to enforce them *a posteriori*.

In the case of chiral invariance, our vector-meson interaction lagrangian is very similar to that of Fujiwara *et al.* [11]), who treat the vector mesons as gauge bosons of hidden local $U(3)_V$ local symmetry of a non-linear $U(3)_L \times U(3)_R$ global chiral-symmetric langrangian. We do not, however, have the "contact" terms which arise in the non-linear model, so that chiral symmetry is slightly broken by the interaction, as well as by the pseudoscalar mass terms. The derivative coupling of the scalar mesons is chiral-symmetric. Again, as with crossing symmetry, we rely on nature for at least a partial restoration of the symmetry.

Although one could take the chiral lagrangian of ref. [11]) and unitarize it according to our prescription - including attaching phenomenological form factors to the contact terms, that would be contrary to the intent of the non-linear chiral lagrangian as an effective lagrangian to be used at the tree level. To go beyond the tree level and maintain chiral invariance, one would have to employ the machinery of chiral perturbation theory [12]) as done by Donoghue *et al.* [8]) in the SU(2) sector using a lagrangian containing only powers of the pion field and its derivatives. Unitarity then becomes a problem, since the one-loop approximation generates only the trivial unitarization of the tree-level approximation, so that resonant amplitudes are poorly described, which adds to the practical problem of the method being far too cumbersome for the applications we envision. In passing we note that, in the limit of $m_\pi \to 0$, the lagrangian used by Donoghue can be obtained from that of Bando *et al.* [13]) (which is the SU(2) version of the lagrangian of Fujiwara *et al.*) taken in the limit of large N_c [ref. [14])].

3.2. CHOICE OF PARAMETER VALUES

Coupling constants, form factor parameters, and bare masses employed in this work are shown in table 1 for $\pi\pi$, and in table 2 for $K\pi$ scattering. All coupling constants in vector meson-exchange processes are related by SU(3) symmetry to the $\pi\pi\rho$ coupling, which is determined from the empirical $\pi\pi$ data. Further couplings involving the scalar (ε, κ) and the tensor (f_2) mesons are independently adjusted to the data. Note that since we do not consider both ε_8 and ε_1, our ε effectively represents a sum of both contributions, in contrast to the κ, which is pure octet. Thus it is not surprising that the resulting ε coupling is larger than the κ coupling. Furthermore, since both scalar couplings involve the mass, symmetry breaking of the order of (m_K/m_π), or even $(m_K/m_\pi)^2$ should also be expected [15]).

The cutoff masses in t-channel processes are adjusted to the scattering data. All values turn out to be rather large; i.e., the data require essentially pointlike couplings. This is especially true for the direct $K\bar{K}$ interaction, which has to be sufficiently

TABLE 1

Parameters used in the t- and s-channel interaction for $\pi\pi$ scattering. In the first column we show the corresponding graphs and in the second one the isospin (I) and isospin factor (IF) with which the two-body matrix elements have to be multiplied. The coupling constants which were used are given in column 3 (for details see the discussion in the text). The numbers in column 4 refer to the different form factors defined in eqs. (2.17)-(2.19) and the corresponding cut-off parameter (Λ) are given in column 5.

Graph	I	IF	$g_1g_2/4\pi$	$F_\alpha(\vec{q}^2)$	$\Lambda[MeV]$
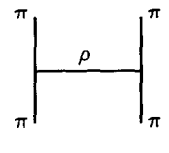	0	-2	2.1	1	1600
	1	-1			
	2	1			
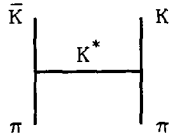	0	$\sqrt{6}$	0.525	1	3000
	1	2			
	2	0			
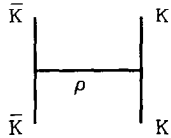	0	-3	0.525	1	4500
	1	1			
	2	0			
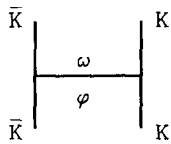	0	1	-0.525 -1.05	1	4500
	1	1			
	2	0			
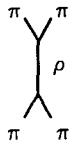	0	0	2.1	2	3000 $m^0 = 1077$
	1	-2			
	2	0			
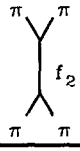	0	3	0.035	3	3000 $m^0 = 1893$
	1	0			
	2	0			
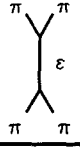	0	3	S 120.	2	3000 $m^0 = 1300$
	1	0			
	2	0	G 0.013	3	3000 $m^0 = 4000$

TABLE 2

Parameters used in the t- and s-channel interaction for $K\pi$ scattering. The notation is the same as in table 1

Graph	I	IF	$g_1g_2/4\pi$	$F_\alpha(\vec{q}^2)$	$\Lambda[MeV]$
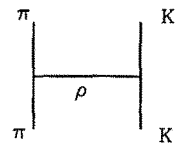	$\frac{1}{2}$	-2	1.05	1	$\Lambda_{KK\rho} = 4500$
	$\frac{3}{2}$	1			$\Lambda_{\pi\pi\rho} = 1600$
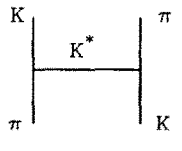	$\frac{1}{2}$	-1	0.525	1	3000
	$\frac{3}{2}$	2			
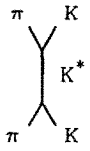	$\frac{1}{2}$	-3	0.525	2	3000
	$\frac{3}{2}$	0			$m^0 = 1077$
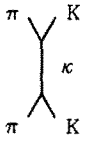	$\frac{1}{2}$	3	S 30.	2	3000 $m^0 = 1400$
	$\frac{3}{2}$	0	G 0.0008	3	3000 $m^0 = 1600$

strong in order to reproduce the characteristic jump of the phase shift in the $\pi\pi$ 0^+ channel. Cutoff masses in s-channel processes are set at 3 GeV. All bare masses are then determined by the fit to the data. In fact, the results for m_0 depend strongly on the choice of Λ, and there is a wide range of (Λ, m_0) values leading to acceptable fits of the data. For example, in case of ρ-exchange, the combinations $\Lambda = 2$ GeV, $m_0 = 966$ MeV and $\Lambda = 4$ GeV, $m_0 = 1350$ MeV lead to equally acceptable descriptions of the data. In other words, each value of m_0 between those two limits is possible, with a suitable choice of Λ. Thus, a better determination of m_0 would require a precise knowledge of the strong $\pi\pi\rho$ form factor.

In principle, all s-channel meson exchanges should appear also as t-channel exchanges in order to satisfy crossing symmetry, even though the form factors and

the unitarization prescription break crossing symmetry. However, it was found in the course of the calculations that the t-channel exchange of the f_2, ε, and κ mesons, because of their high mass and the type of coupling, had negligible effects on the results in the range of energy investigated. They were therefore omitted as a matter of calculation convenience. At higher energies they would have to be included.

More serious, however, is the absence of an explicit contribution to the quasipotential arising from the exchange of $\pi\pi$ systems with c.m. energies in the range of $2m_\pi$ to ~ 1 GeV, presumably in a relative s-wave (the so-called σ-channel). Since the $I=0$ s-wave amplitude is not small, the effects should be appreciable. Within the model this low-mass 2π exchange contribution could be generated by diagrams which present two ρ-mesons in the s-channel. Evaluation of the 2π-2ρ box diagram, for example, gave a small but non-negligible contribution to most amplitudes.

4. Pion–pion scattering

4.1. ROLE OF ρ-EXCHANGE

We start with the $I=J=1$ and $I=2$, $J=0$ phase shifts which both serve to pin down the ρ contribution, in the s- as well as in the t-channel. This is possible because the coupling to the $K\bar{K}$-channel does not play any role here - for several reasons: first, the $K\bar{K}$ system cannot be in an $I=2$ state; second, the coupling to the $K\bar{K}$ channel leads to very short-ranged contributions (of second order in K* exchange) in the $\pi\pi$ channel, so that essentially only s-waves are affected. In addition, the direct $K\bar{K}$ interaction, because of strong cancellations between ρ- and ω-exchange in the $I=J=1$ channel (see table 1), is quite weak there.

The resonant behavior in the $I=J=1$ channel requires the inclusion of s-channel ρ-exchange in the interaction. If only the pole contribution (fig. 3c) is taken into account, we have, in essence, a Lee model [16]), with the benefit of everything being finite due to the use of form factors. Unitarization of the scattering amplitude via the scattering equation (eqs. (2.9)-(2.12)) will cause the resonance in the amplitude which is generated by the pole in the quasipotential to be shifted considerably from the position of the quasipotential pole, and the resonance will acquire a width as well. We can speak of the location of the pole in the potential as the "bare" mass (m_0) of the particle, and the location of the resonance in the physical amplitude as the "renormalized" or "dressed" mass (m) of the physical particle.

This Lee model has to be extended by including the negative-energy contribution of the s-channel process (fig. 3d) and t-channel ρ-exchange. (The presence of the latter contribution is dictated by various other partial wave phase shifts; see below.). The scattering equation is then solved numerically and m_0 and $g^2_{\pi\pi\rho}$ are adjusted to the empirical δ^1_1 phase shifts. We show the results in figs. 4 and 5 for the imaginary part of the amplitude and for the phase shift. The inclusion of the process of fig. 3d shifts the Lee model result for the mass very slightly and leaves the width virtually

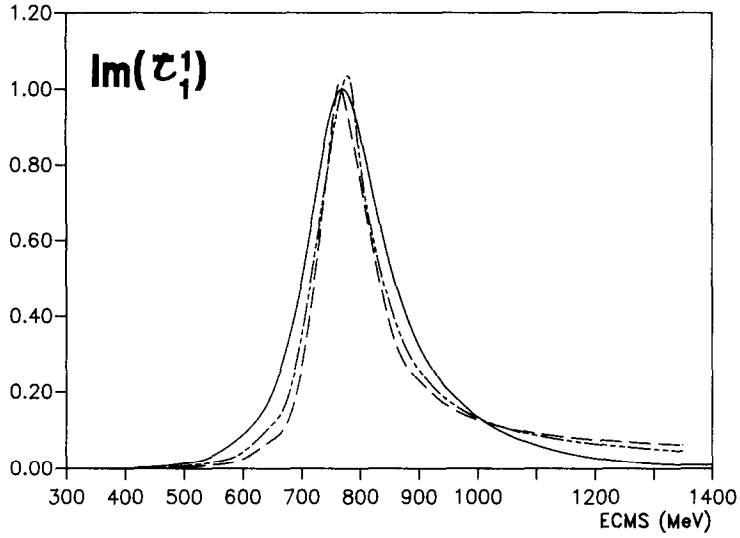

Fig. 4. The imaginary part of the $I = 1$, $J = 1$ partial wave amplitude, showing the effect of various processes. The long-dashed curve shows the effect of the s-channel pole alone in the quasipotential. The dot-dashed curve shows the effect of including the contribution of fig. 3d. The strong enhancement of the width of the physical resonance due to t-channel contributions is shown by the solid curve.

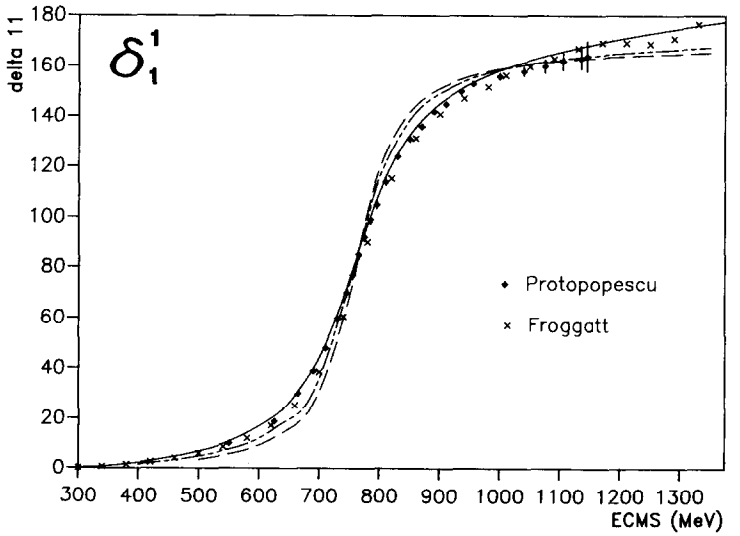

Fig. 5. The same effects as in fig. 4 for the δ_1^1 phase shift, compared with results of two phase-shift analyses, refs. [17,18]).

unchanged. Turning on the t-channel "background" interaction has, however, a significant effect. Whereas the position of the resonance is shifted only slightly - to a lower energy, as expected, since t-channel ρ-exchange is attractive in this channel, the width is increased by approximately 50%. This is the reason why our $\pi\pi\rho$ coupling constant is correspondingly smaller than the value deduced from the width of the physical particle (2.1 compared with 2.94). Similar effects, often more dramatic, occur in other pole-driven channels (see table 3). Note that the presence of t-channel ρ-exchange also affects the size of the other contributions since all SU(3) predictions of coupling constants are based on $g^2_{\pi\pi\rho}/4\pi = 2.1$.

The $I = 2, J = 0$ phase shift is used to fix the cutoff mass Λ at the $\pi\pi\rho$ vertex in the t-channel. (An s-wave is needed since it is most sensitive to variations of the cutoff parameter). In fact, the repulsive nature of the phase shifts in this channel definitely requires t-channel ρ-exchange. With $\Lambda = 1700$ MeV, the theoretical results reproduce the data well as long as the two analyses agree (see fig. 6). At least the data of Froggatt *et al.* [17]) seem to indicate that the $\pi\pi$ interaction has to be less repulsive beyond 800 MeV. The missing attraction at higher energy might be connected with the contribution of the correlated $\rho\rho$ channel, which we have not yet considered.

Having fixed all parameters in (s- and t-channel) ρ-exchange, we now make a prediction for the $I = J = 2$ phase shift. Again, t-channel ρ-exchange is the only piece that can contribute and, indeed, leads to perfect agreement with the empirical phase shifts (see fig. 7).

4.2. THE f_2 MESON

Apart from a small effect due to t-channel ρ-exchange, the $I = 0, J = 2$ channel is dominated by an explicit resonance in the s-channel - the $f_2(1270)$ meson. In

TABLE 3

Bare (m_0), renormalized (m, m_L) masses and widths Γ, Γ_L for the s-channel resonances used in the present paper; m and Γ are the empirical values, which agree with the results from the complete calculation; m_L and Γ_L are obtained when the t-channel interaction is turned off. The upper and lower values for ε and κ correspond to scalar and derivative coupling, respectively

Meson	m	Γ	m_0	m_L	Γ_L
ε	1400	150–400	1300	1335	600
			4000	4850	650
κ	1429	287	1400	1380	260
			1600	146	46
ρ	769	153	1077	813	109
K*	892	51.3	1077	921	32
f_2	1274	185	1893	1391	170

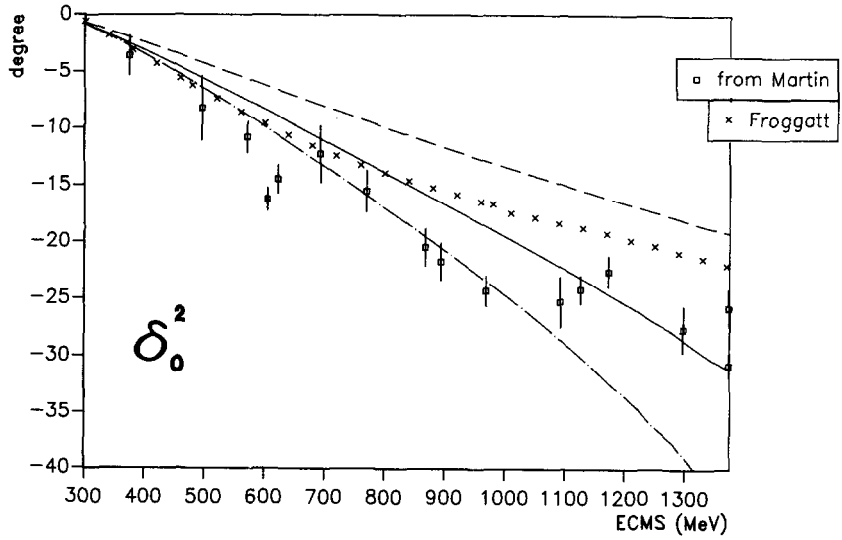

Fig. 6. The $I=2$, $J=0$ $\pi\pi$ phase shift, obtained from t-channel ρ-exchange, for various cutoff-masses Λ (solid line: $\Lambda = 1700$ MeV, dashed line: $\Lambda = 1300$ MeV, dash-dotted line: $\Lambda = 2100$ MeV). The empirical analyses are those of refs. [17,19]).

order to reproduce the experimental phase shift shown in fig. 8 we have to introduce a meson of $m_0 = 1895$ MeV (based on $\Lambda_{\pi\pi f_2} = 3.0$ GeV) that produces a resonance at $m = 1274$ MeV with a width of 185 MeV (cf. table 3).

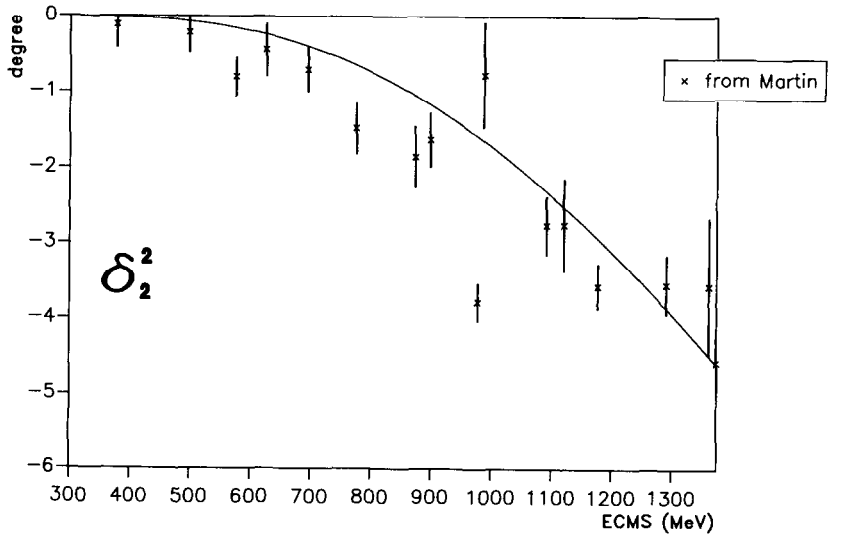

Fig. 7. The $I=2$, $J=2$ $\pi\pi$ phase shift compared with the data from ref. [19]).

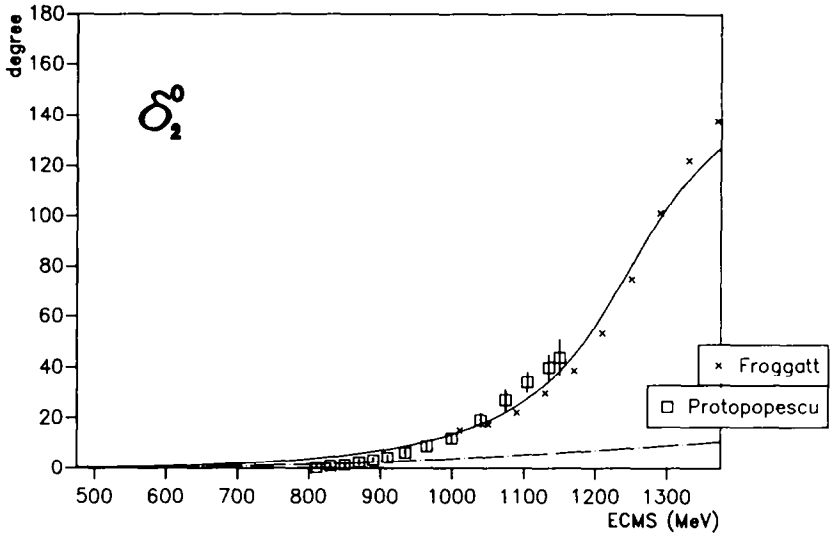

Fig. 8. The $I = 0$, $J = 2$ phase shift. The dot-dashed curve shows the result with only t-channel exchange. The solid curve shows the result when the f_2 meson is included as an s-channel contribution in the potential. The data are taken from refs. [17,18]).

4.3. THE SCALAR-ISOSCALAR CHANNEL $I^G(J^{PC}) = 0^+(0^{++})$

We finally come to the most interesting channel, with quantum numbers $I^G(J^{PC}) = 0^+(0^{++})$. The experimental $\pi\pi$ phase shift in this channel (δ_0^0) shows a 180° jump in a narrow energy range around $E \simeq 980$ MeV. This resonance (S*(975)) was originally interpreted as a member of the scalar $q\bar{q}$ nonet. Jaffe [20]) has pointed out that this interpretation leads to difficulties and suggested that S*(975) and $f_0(980)$ might be four-quark states (two-quark-two-antiquark), whereas the genuine $q\bar{q}$ scalar mesons should be several hundred MeV higher in energy. We will show that in our model the spectrum below 1 GeV is essentially given as a correlated two-pion and two-kaon system. Similar conclusions have been obtained by Weinstein and Isgur [21]) from quark model calculations and by Barnes [22]) from a study of two-photon decays.

4.3.1. Omitting the $K\bar{K}$ interaction. In order to demonstrate the outstanding role of the direct $K\bar{K}$ interaction in the present results, we first leave out this contribution. That is, we solve eq. (2.12) with the effective potential $\tilde{V}_{11}$ in the $\pi\pi$ channel consisting of (t-channel) ρ-exchange plus the second-order box diagram involving the $K\bar{K}$ intermediate state, as shown in fig. 9a. As demonstrated in fig. 10 for δ_0^0, both contributions are quite small and cannot account at all for the observed resonance behavior around 1 GeV. In order to obtain agreement with the empirical situation, one may include a genuine scalar meson in the s-channel (pole graph), the coupling parameters and mass of which are appropriately chosen. We mention that such a procedure has been previously used in refs. [6,7]), but with omission of

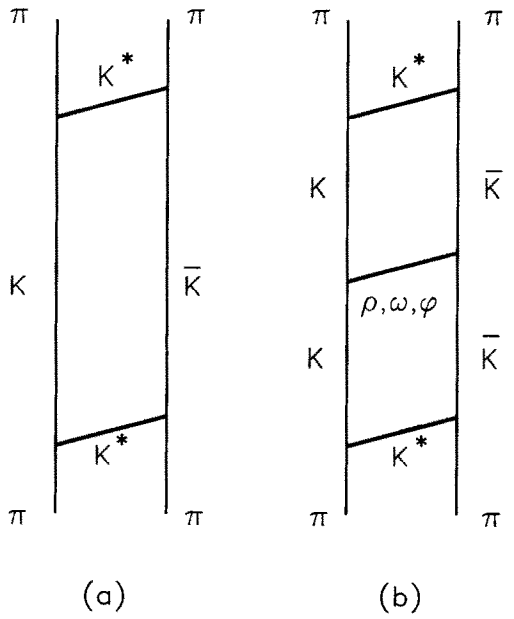

Fig. 9. Coupling of the $\pi\pi$ and $K\bar{K}$ channels by K* exchange. (a) includes the $K\bar{K}$ box diagram only whereas (b) takes in addition the direct $K\bar{K}$ interaction into account.

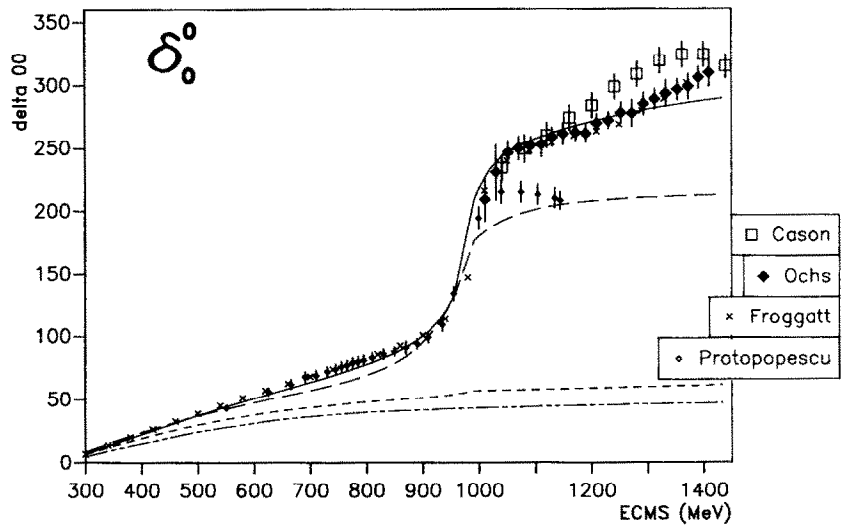

Fig. 10. The predictions of four different models for the $I=0$, $J=0$ $\pi\pi$ phase shift. The dot-dashed curve is the result for ρ-exchange only. The short-dashed curve includes the effect of coupling to the $K\bar{K}$ channel with no diagonal $K\bar{K}$ interaction. The long-dashed curve includes strong t-channel exchange contributions in the $K\bar{K}$ channel (model I). The solid curve adds the ε as an s-channel process, with derivative coupling (model II). Experimental phase shifts are taken from refs. [17,18,23,24]).

the t-channel interaction. The inclusion of $K\bar{K}$ box diagrams leads to the required decrease of the $\pi\pi$ flux beyond the $K\bar{K}$ threshold. The theoretical prediction, however, does not quite reproduce the experimental situation, as shown in fig. 10 (short-dashed line).

4.3.2. Full coupled-channels approach. As table 1 shows, the t-channel interaction between $K\bar{K}$ pairs for $I = 0$ is rather strong and attractive because all contributions add coherently. Therefore we expect a much larger effect from the $K\bar{K}$ channel if we take this interaction into account by solving eq. (2.9) simultaneously for $\pi\pi$ and $K\bar{K}$. The effect on the phase shift due to this channel is indeed very strong, as demonstrated in fig. 10 (long-dashed line). We observe a rapid increase in the phase shift which comes from a quasi-bound $K\bar{K}$ pair. Because of the attractive interaction in the t-channel, this state is shifted by several MeV below threshold, which gives rise to a strong resonance-like behaviour in the phase shift. In fig. 11 we observe that the inclusion of the direct $K\bar{K}$ interaction leads only to a minor modification of the elasticity η_0^0. It is important to mention that so far only t-channel interactions have been taken into account. We refer to this as model I. We do not need to introduce a genuine scalar resonance around 1 GeV in order to reproduce the experimental phase shifts from the $\pi\pi$ threshold up to 1 GeV. Beyond 1 GeV, however, the theoretical results deviate qualitatively from the more recent experimental phase-shift analyses. The data clearly indicate an additional resonance behavior that we will investigate in the next section.

4.3.3. The genuine scalar meson. As we explain the phase jump at 980 MeV as being due to a quasi-bound $K\bar{K}$ pair, it is obvious that the further increase of the

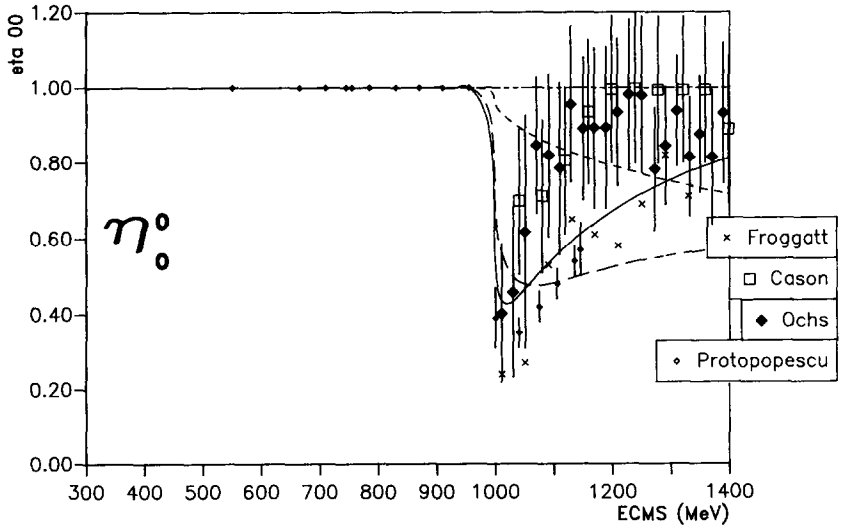

Fig. 11. The predictions of four different models for the elasticity parameter in the $I = 0$, $J = 0$ $\pi\pi$ channel. The various curves correspond to those in fig. 10. Experimental information is taken from refs. [17,18,23,24]).

phase beyond 1 GeV, in view of the absence of important open channels in that region, should be connected with the genuine scalar mesons which belong to the scalar SU(3) nonet - one a member of the octet and the other a singlet. The particle data group [25]) lists a scalar meson $f_0(1400)$ (the previous $\varepsilon(1300)$)at 1400 MeV with a width of 150–400 MeV that decays mainly into two pions. We introduce in the following a scalar meson (which we refer to as the ε meson), the bare mass and the coupling constant of which we take as free parameters that are adjusted to fit the experimental phase shifts beyond 1 GeV. The corresponding cutoff mass is set to 3 GeV.

Of course, one can couple the scalar meson in various ways to the pion: one way is the usual scalar coupling; the other possibility is the derivative coupling (see eq. (2.4)). The two couplings lead to quasipotentials with quite different properties. In contrast to the scalar coupling, the derivative coupling increases strongly with the pion momentum above 1 GeV and gives rise to a quasipotential which hardly alters the phase shifts below 1 GeV. Since model I already describes the data up to 1 GeV satisfactorily the derivative coupling seems to be preferred. Indeed, if we add the ε meson with this coupling (model II), good agreement between theory and experiment is obtained throughout the whole energy range cf. figs. 10, 11). The bare mass and the coupling constant (which is directly connected with the width) of the ε meson has been chosen to reproduce the high-energy data of Ochs [23]) and Froggatt *et al.* [17]), leading to a physical mass of about 1400 MeV and a width of approximately 400 MeV, as estimated from an Argand speed profile. (The inelasticity renders a more precise determination of the mass and width impossible). The resulting values for the η_0^0 parameter lie between the experimental data points of Ochs and those of Froggatt which have, unfortunately, large error bars. Nevertheless, it appears that not only the phase shifts but also the inelasticities calculated with model II are in better agreement with the experimental data than those of model I.

The difference between scalar and derivative coupling is nicely demonstrated by a Lee model calculation based on (s-channel) ε-exchange. Corresponding results for the δ_0^0 phase shift are shown in fig. 12. In the case of scalar coupling, the strong attractive interaction in the low-energy range would destroy the already good agreement between theory and experiment provided by model I. However one can restore the good results without eliminating the improvement at higher energies if one introduces a very short-ranged repulsive contribution, which we parametrize here by (s-channel) scalar-meson exchange of opposite sign. The mass of this inverted-sign scalar meson is set to 4 GeV and the coupling parameters are adjusted until the experimental scattering length a_0^0 is reproduced. The results for δ_0^0 and η_0^0 derived from such a model (II') are shown in fig. 13. Obviously, the agreement with experiment is as satisfactory as before, although the predictions of models II and II' differ somewhat around 1.1. GeV.

Of course, such a repulsive contribution is in some sense an unpleasant feature because it cannot be easily justified in the meson-exchange framework. On the other

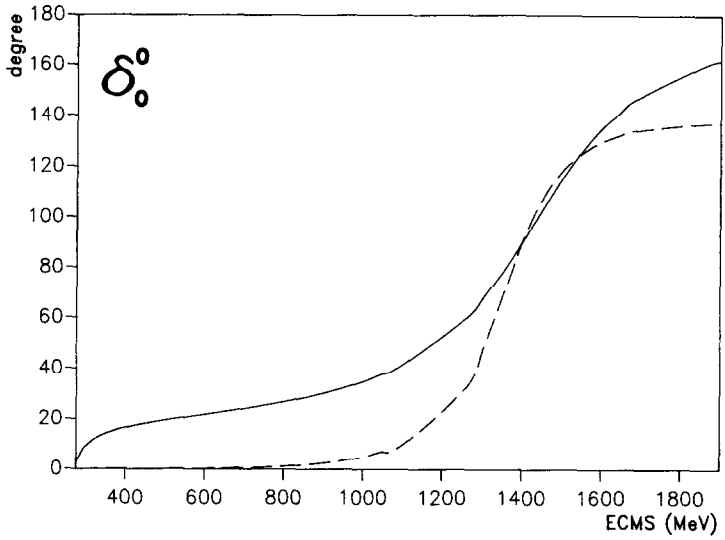

Fig. 12. The $I = 0, J = 0$ phase shift due solely an s-channel pole (ε meson) in the potential. The solid curve is for scalar coupling; the dashed curve is for derivative coupling. Bare masses and coupling constants have been adjusted to produce a phase shift of 90° at 1400 MeV. The cutoff mass Λ is set at 3 GeV.

hand, it might be an indication of quark-gluon effects, i.e. phenomena beyond the meson-exchange picture.

In any case, whether the derivative coupling (model II) or the scalar coupling plus phenomenological repulsion (model II′) is nearer to the physical reality remains to be clarified.

Finally, we compare in fig. 14 the calculated transition phase shifts $\delta_{12}(I = J = 0)$ for $\pi\pi \to K\bar{K}$ with the experimental ones. These represent a real test for our models because all parameters have been fixed from foregoing studies. Indeed, model II provides a good description of the empirical data. Obviously both the strong direct $K\bar{K}$ interaction and the genuine ε meson are needed to obtain agreement with experiment.

4.4. SCATTERING LENGTHS

Since, in general, none of the resulting scattering lengths has been fitted to the experimental data (with the exception of a_0^0 in model II′), the experimental values provide another test of our interaction model at low energies. In table 4 our results are compared with the experimental data. As in the a_0^2 and a_2^2 case no s-channel resonances exist; the scattering length is completely generated by the t-channel interaction. As discussed before in the case of derivative coupling, the influence of the ε-meson on the scattering length a_0^0 is weak compared with the other t-channel interactions. On the other hand, the influences of the ρ-meson on a_1^1 is very strong

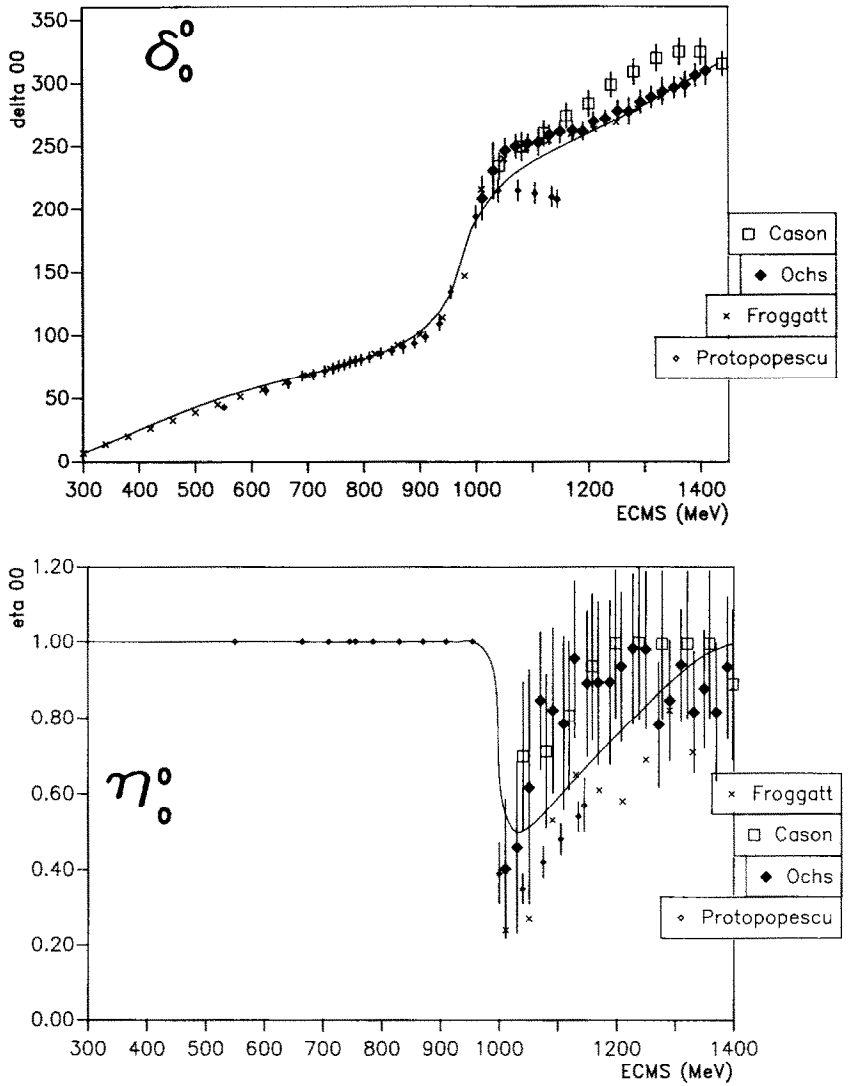

Fig. 13. The $I=0, J=0$ $\pi\pi$ phase shift (a) and elasticity parameter (b) calculated with model II′, which contains t-channel exchanges, coupling to $K\bar{K}$ with strong $I=0$ $K\bar{K}$ interaction, and an s-channel scalar meson (ε) with scalar coupling plus a *repulsive* scalar term of short range to compensate the scalar attraction at low energy. The experimental phase shifts are taken from refs. [17,18,23,24]).

because the resonance is relatively low in energy. In the case of a_2^0, the contributions of the t-channel interactions and of the f_2 meson are about equally strong. Obviously the overall agreement between the theoretical and experimental scattering data is good, especially if we bear in mind that these data have not been used in the adjustment of the model parameters.

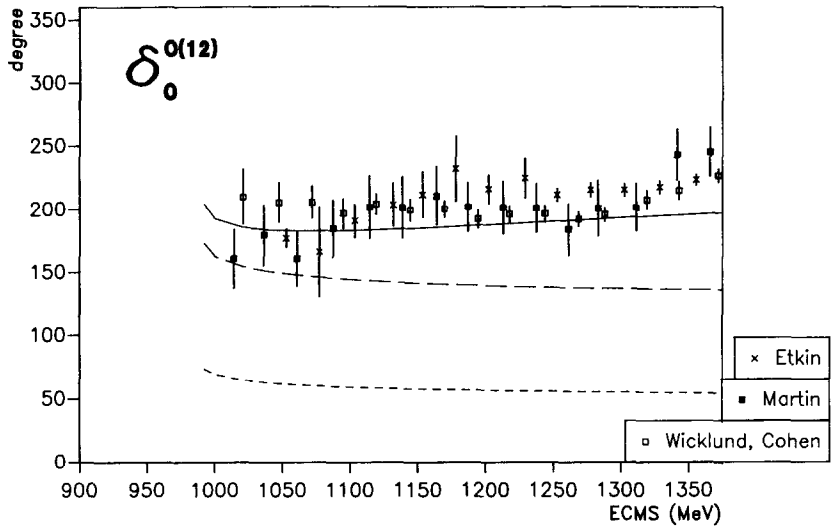

Fig. 14. The transition phase shift for $\pi\pi$-K$\bar{\text{K}}$ in the $I=0$, $J=0$ partial wave calculated with model II. The long-dashed curve shows the result when the ε-meson is omitted whereas the short-dashed curve is obtained when, in addition, the diagonal K$\bar{\text{K}}$ interaction is suppressed. Experimental phase shifts are taken from refs. [26-29]).

We remind the reader that below 1 GeV all amplitudes but for the $I=0$ s-wave are driven solely by t- and s-channel single vector-meson exchange; no explicit $I=0$ t-channel contribution of range <1 GeV^{-1} appears in the quasipotential. Based on our experience with the coupling to the K$\bar{\text{K}}$ channel, it is possible that an equivalent treatment of the $\rho\rho$ channel (see sect. 3.2) could supply much of the absent low-mass isoscalar t-channel exchange. However, at this point in the development of the

TABLE 4

Experimental and theoretical scattering lengths for $\pi\pi$ (upper part) and $K^-\pi^+$ (lower part) scattering. The experimental data are taken from ref. [30]). In the Kπ case we have chosen these data which were available for all three scattering lengths from the same group. The results shown in the last column were obtained from model I leaving out the pole term in the s-channel

a_j^i	Experiment	Model I	Model II	No resonance
a_0^0	0.26 ± 0.05	0.31	0.32	
a_0^2	-0.028 ± 0.012	-0.027		
a_1^1	0.038 ± 0.002	0.040		0.008
a_2^0	$(17 \pm 3) \times 10^{-4}$	9.1×10^{-4}		5.3×10^{-4}
a_2^2	$(1.3 \pm 3) \times 10^{-4}$	-2.6×10^{-4}		
$a_0^{1/2}$	0.24 ± 0.002	0.23	0.24	
$a_0^{3/2}$	-0.05	-0.064		
$a_1^{1/2}$	0.018 ± 0.002	0.018		0.005

model it is clear that the effects of this missing contribution are being absorbed in the parametrization of the vector-meson exchange.

4.5. CROSS SECTIONS AND Y-MOMENTS

All of the fitting that we have done has been to the phase shifts extracted by various authors [17,18,23]) from scattering data. We have not attempted to achieve a best statistical fit to the total set of phase shifts and scattering lengths, but have simply adjusted the parameters "by hand" to get an approximate best fit. The danger in this is, of course, that small deviations from the experimental phase shifts in different partial waves can add coherently, so that an apparently good fit to several phase shifts may not produce nearly as good-looking a fit to the actual experimental data. Here we examine the fit of our model to cross sections and to the Y-moments [18]) for $\pi\pi$ scattering.

The data for $\pi^+\pi^-$ total cross section and the result of our model is shown in fig. 15. In general, the fit of the model to the cross section is as good as the fit to the different phase shifts. The slight deviation in the 1.0–1.15 GeV energy region (just above the $K\bar{K}$ threshold) is consistent with the discrepancy between the model's prediction for the $I=0$ s-wave phase shift and the s-wave phase shift of the Protopopescu *et al.* [18]) analysis. The cross section for $\pi^+\pi^- \to K\bar{K}$ is shown in fig. 16. Our model undershoots the data of Protopopescu, just as expected from the fit to the elasticity parameter - our η_0^0 is somewhat closer to unity than that of Protopopescu, but in better agreement with later analyses [17,23]). Since the only open

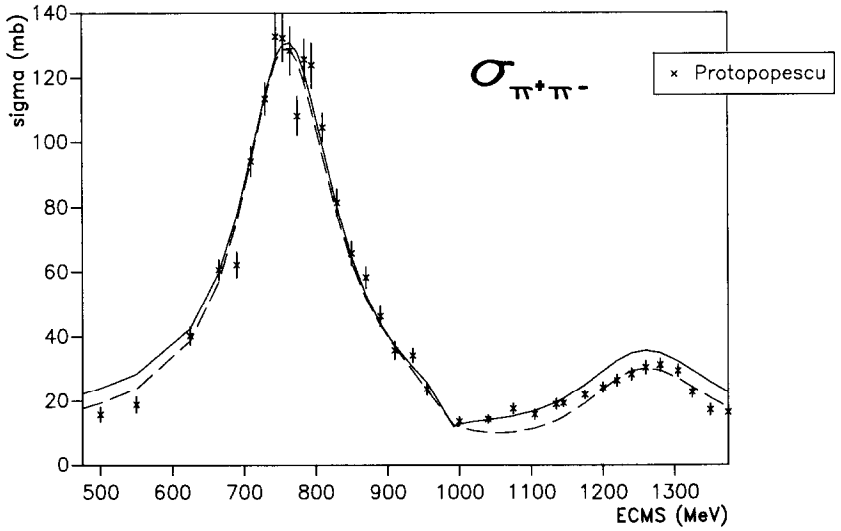

Fig. 15. The $\pi^+\pi^-$ total cross section computed with model I (dashed curve) and model II (solid curve). The data are from refs. [18]).

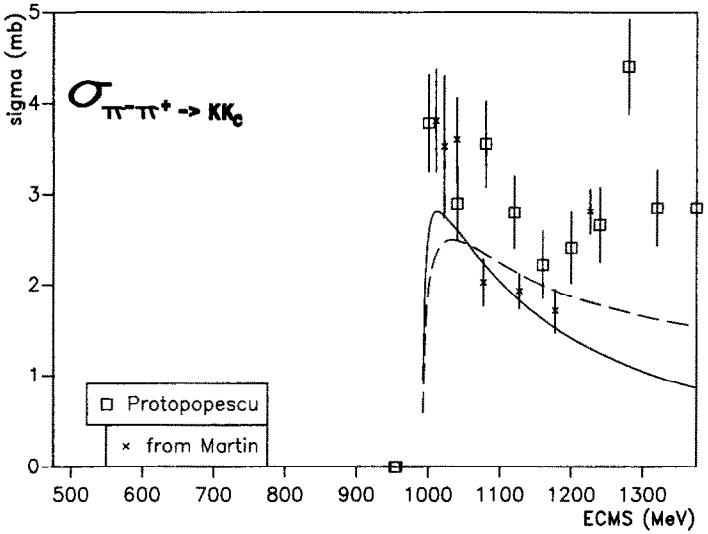

Fig. 16. The total cross section for $\pi^+\pi^- \to K\bar{K}$ calculated with model I (dashed curve) and model II (solid curve) compared with the data of refs. [17,18]).

channel we have considered is the $K\bar{K}$ s-wave, this is not surprising. Protopopescu's analysis includes some inelasticity in three partial waves. Inclusion of the $K\bar{K}$ channel in other partial waves in our calculation could make enough difference in the relatively small inelastic cross section to achieve a substantially better fit.

For the sake of completeness, comparison of the model's predictions for the Y-moments for $\pi^+\pi^-$ elastic scattering (for definitions see ref. [18])), which gives some indication of the fit to the differential cross section, are shown in fig. 17. The differences here, especially those above 1.0 GeV, which are directly traceable to the discrepancies between our phases and elasticities and the Protopopescu analysis, are not unexpected. Since the moments at higher energies become especially sensitive to d-, f- and higher partial waves, and we have included no $I=1$, $J=3$ or higher resonances, the discrepancies are not surprising. We note in particular the behavior of Y_3^0, which is particularly sensitive to f-waves.

5. Kaon–pion scattering

Our model for the $\pi\pi$ interaction can now be extended in a straightforward way to the $K\pi$ system. This system is of special interest since a considerable part of our model for the $K\pi$ interaction, namely the t-channel exchange contributions (see fig. 2), are completely determined by the previous study of the coupled ($\pi\pi$, $K\bar{K}$) system. Only additional pole contributions in the s-channel have to be adjusted separately.

We start with the $I=\frac{1}{2}$, $J^P=0^+$ channel of the $K\pi$ system, which is the analog of the $I=0$, $J^P=0^+$ wave in the $\pi\pi$ system. (Note that kaons have isospin $\frac{1}{2}$ and

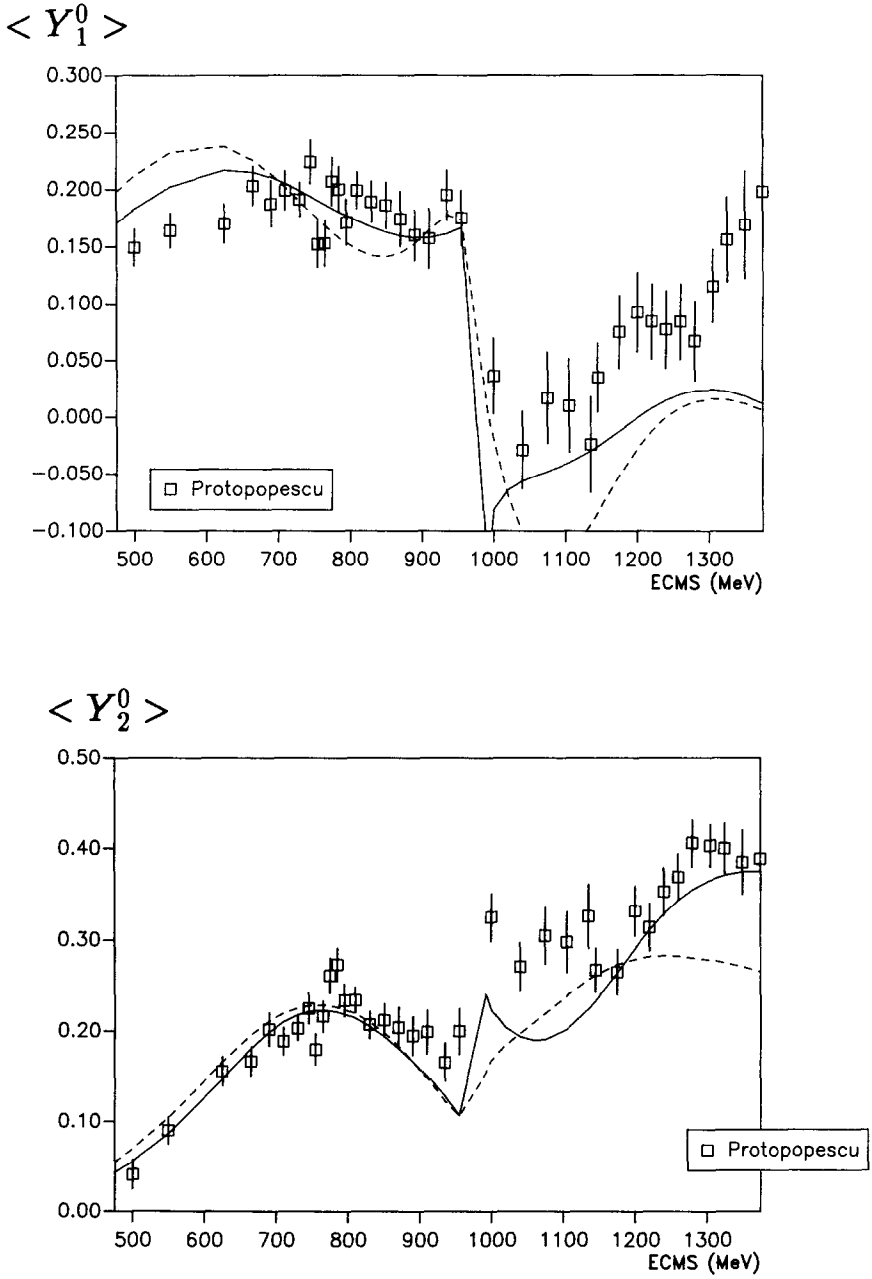

Fig. 17. The Y-moments calculated with model I (dashed curve) and model II (solid curve). Empirical values are taken from the analysis of ref. [17]).

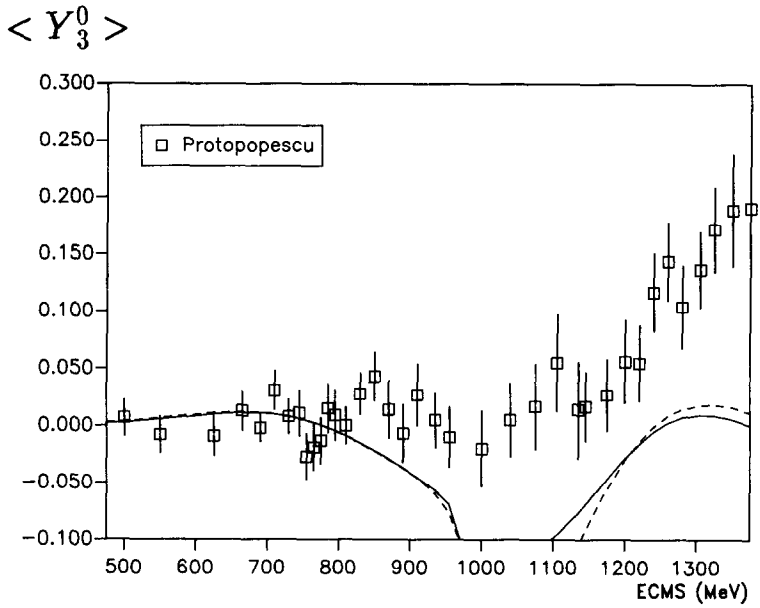

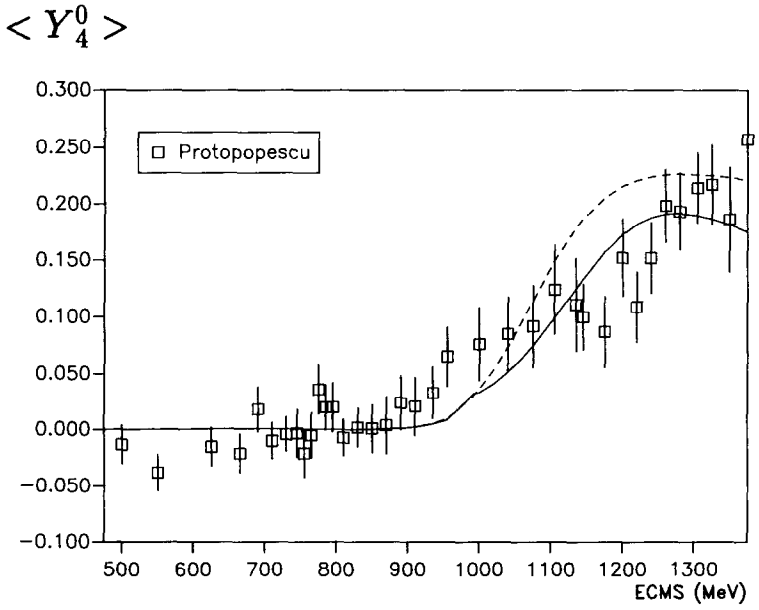

Fig. 17—continued

no definite G-parity.) In addition to the older phase shift analyses [31-33]) there are now very high-statistics data [36]) for this channel. In a first step, we include the t-channel interaction (ρ, K*-exchange) only (model I). As fig. 18 demonstrates, it is by far the most important part of the Kπ interaction below 1 GeV. In contrast to the $\pi\pi$ case, there is no appreciable channel coupling: the only possible open channel below 1.5 GeV is the Kη system, which can be neglected because of the weak diagonal interaction. On the other hand, similar to the $\pi\pi$ case, there are strong deviations of the predictions of model I from the experimental phase shifts above 1 GeV, which again require the introduction of a genuine scalar meson (the analog of the ε meson discussed in sect. 4.3). This meson, with strangeness and $I(J^P)=\frac{1}{2}(0^+)$, is usually denoted as κ. We mention that the scalar channel of the Kπ system is actually simpler than the $\pi\pi$ system because here we expect only one single-meson resonance: the member of the scalar octet.

Again we have the ambiguity of coupling the scalar meson κ to the two pseudoscalar mesons K, π: one can either use scalar or derivative coupling. Based on derivative coupling and a bare κ mass of 1.6 GeV, the sum of t-channel interactions and κ pole graph leads to the result shown in fig. 18. The corresponding physical κ-mass is 1430 MeV with a width of $\Gamma \approx 300$ MeV. The nearly perfect agreement between the experimental and theoretical $\delta_0^{1/2}$ phase shift strongly supports our model. We should, however, also bear in mind that channel coupling may become important around 1.5-1.6 GeV where the ρK* and ωK* thresholds lie. Investigations of these effects are in progress.

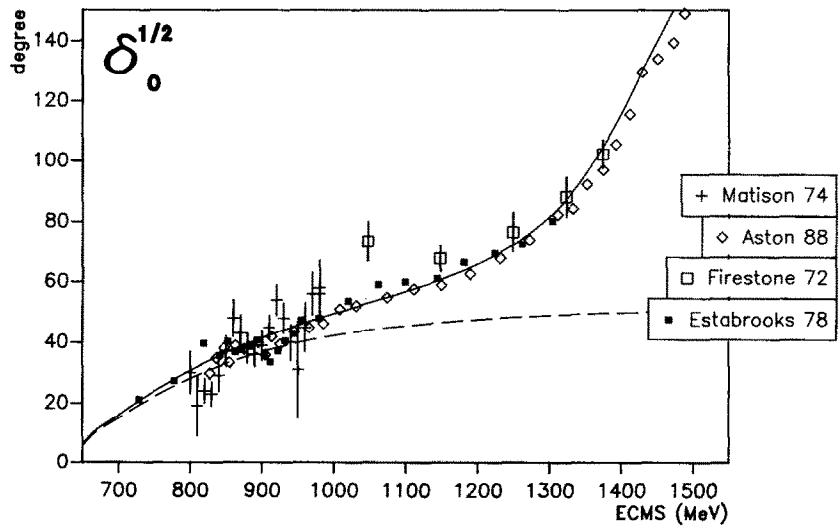

Fig. 18. The $I=\frac{1}{2}, J=0$ Kπ phase shift calculated with model I (dashed curve), which omits the κ meson s-channel contribution, and model II (solid curve), which contains the κ meson contribution with gradient coupling. The data are from the analyses of refs. [31-34]).

Further excellent tests for the meson-exhange interaction in the t-channel are the $\delta_0^{3/2}$ and $\delta_1^{3/2}$ phase shifts. Like the δ_0^2 and δ_2^2 phase shifts in $\pi\pi$ scattering, all of the effects come from the t-channel interaction. The good agreement between theory and experiment shown in fig. 19 indicates that our model of the interactions works

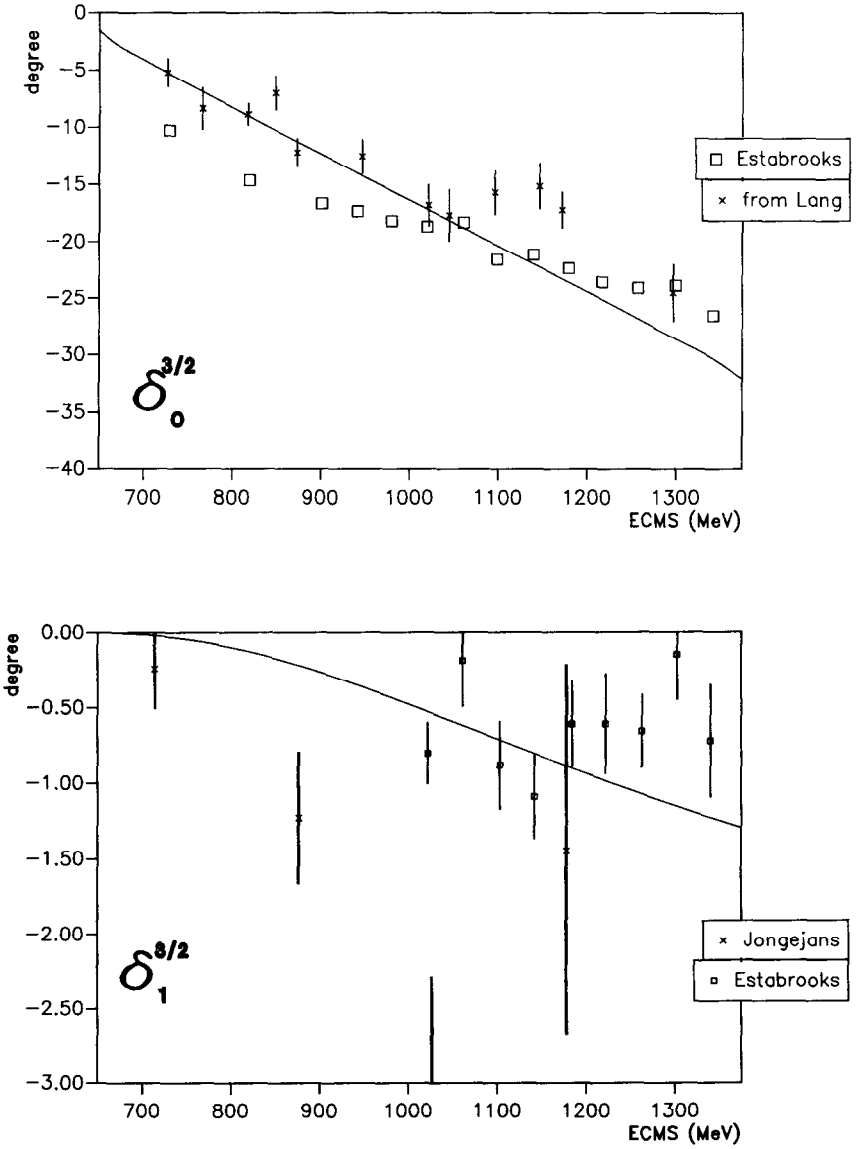

Fig. 19. The $I = \frac{3}{2}$ phase shifts of model I for $J = 0$ (a) and $J = 1$ (b) compared with analyses of refs. [32,36]) and data from ref. [35]). The interaction in these channels is due solely to t-channel meson exchange.

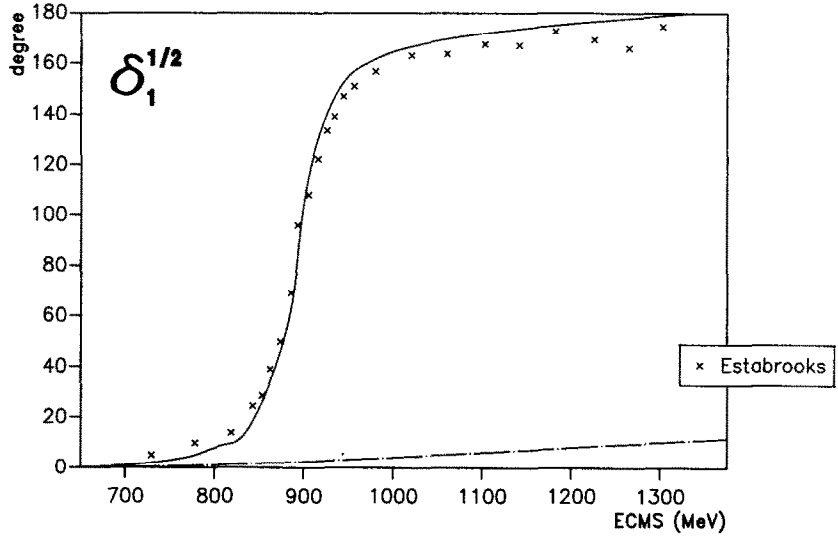

Fig. 20. The $I=\frac{1}{2}, J=1$ Kπ phase shift showing the effect of t-channel exchange alone (dot-dashed curve) and the result of including the K* as a driving term in the potential (solid curve). The data are from ref. [24]).

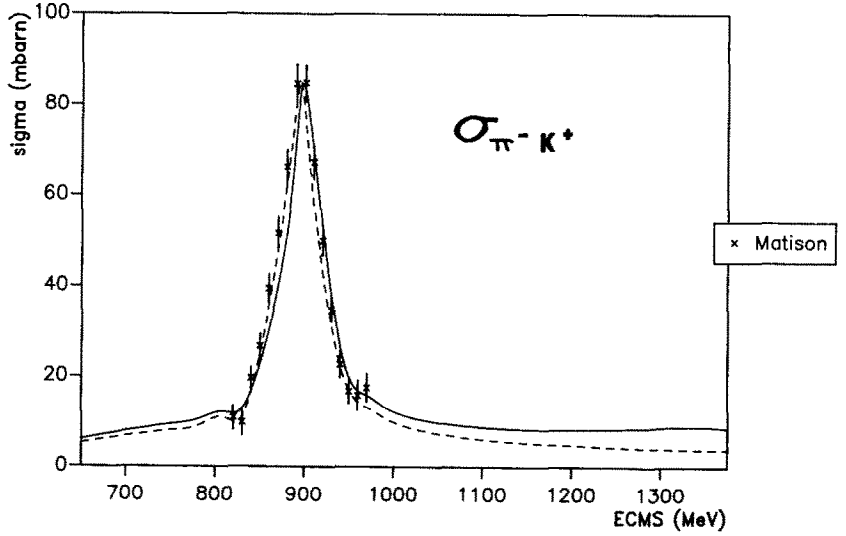

Fig. 21. The $K^+\pi^-$ total cross section calculated with model I (dashed curve) and model II (solid curve). The data are from ref. [31]).

well, especially since all of the relevant parameters have been fixed by the fit in the $\pi\pi$ sector.

The phase shift for the $I=\frac{1}{2}, J=1$ Kπ channel is dominated by the K* resonance, as seen in fig. 20. The excellent fit to the phases in the energy region of the K* results in the excellent overall fit to the $K^+\pi^-$ total cross section shown in fig. 21. The importance of the K* is evident. On the other hand, the bare K* resonance is strongly modified due to the coupling to the Kπ channel, as one can see from table 3. Finally, the predictions for the scattering lengths are again in perfect agreement with empirical information (see table 4).

6. Summary and conclusions

The indications that in the limit of a large number of colors QCD at low energies become a theory of weakly interacting mesons has led us to attempt to explain low energy meson-meson scattering in the framework of meson exchange. The fact that meson-meson scattering amplitudes remain elastic well above the energy threshold for multiple pion production makes the treatment of meson exchange through a quasipotential in a scattering equation possible. Indeed, even after the onset of inelasticity (e.g., the K$\bar{\text{K}}$ channel), the inelasticity occurs mainly in two-body channels, so that much of the effect of inelasticity can be included through the device of channel coupling in the scattering equation.

In the model we have constructed, meson exchanges, both in the s- and t-channels, are the sole driving factors. All the mesons considered in the model are either well-established particles - π, K, η, ρ, ω, K*, η', f_2, φ - or are expected from the quark model - ε, κ - and for which there exists considerable experimental evidence. The coupling constants are consistent in almost all cases with SU(3) symmetry, although the use of physical masses and different form factor parameters results in considerable symmetry breaking in the interaction. However, the form factor parameters, which we view as an expression of the unknown underlying multi-quark effects, are all in the range expected from hadronic sizes, i.e., 1.5–4 GeV.

In our model we consider the pseudoscalar mesons as elementary modes which are described in the underlying quark model as correlated quark-antiquark pairs. The resonances (mesons) in the other channels which we have investigated are of a more complicated structure. There exist, first of all, genuine ("bare") resonances which can be considered as correlated quark-antiquark systems, but in addition there are correlated pairs of pseudoscalar mesons with the same quantum numbers which strongly couple to the genuine resonances. These correlated pairs of pseudoscalar mesons are described in the quark model as two-quark-two-antiquark systems. Due to the coupling to the pseudoscalar mesons, the genuine resonances are strongly shifted in energy. Therefore the bare masses of these resonances are, in general, very different from the physical ones, and lie in all cases beyond 1 GeV. The spectrum below 1 GeV is strongly influenced by the correlated pseudoscalar meson pairs,

whereas in the s-wave $\pi\pi$ and $K\pi$ phase shifts the scalar ε and κ mesons have only little influence on the phases below 1 GeV - provided that derivative coupling is chosen. The jump in the $I=0$ s-wave $\pi\pi$ phase shift turns out to be due to a quasi-bound $K\bar{K}$ pair in our model, with a width of 30 ± 5 MeV.

Application of the model to the $\pi\pi$ and $K\pi$ systems yields an excellent quantitative fit to all the experimentally measured phase shifts in the energy range up to 1.5 GeV, although discrepancies at the highest energies suggest that it may be necessary to include coupling to channels with thresholds slightly above 1.5 GeV. The model can easily be extended to include such channels without introducing additional parameters. While some partial waves require an s-channel pole in the quasipotential, the t-channel exchange processes are found to play an important role in the low energy behavior of the phase shifts and to have substantial influence on the observed widths of the resonances. It is gratifying to note that the partial waves in which resonances are absent and are, therefore, entirely given by t-channel exchange, are also very well described by the model. It is our hope that the model will find use in explaining processes where many of the same vertices occur, e.g. in meson-nucleon interactions, or in interactions requiring a reliable off-shell extrapolation of the meson-meson T-matrix.

Coming back to the questions raised in the introduction, we have shown that, in spite of the absence of strong short-range repulsion, the meson-exchange picture works remarkably well - for the $K\pi$ as well as for the $\pi\pi$ system. Even beyond 1 GeV there is no need for introducing explicit quark effects. Of course, the underlying parameters - coupling constants, bare and cutoff masses - have ultimately to be derived from QCD.

J.D. would like to express his appreciation for the support and hospitality of the Institut für Kernphysik, and to acknowledge the additional support of a Mount Holyoke College Faculty Fellowship. J.S. thanks G.E. Brown, G. Garvey, and M.B. Johnson for discussions and the hospitality he enjoyed at Stony Brook and at LAMPF. Numerous discussions with E.L. Lomon and conversations with W. Dunwoodie and W. Oelert concerning the current experimental status of the interactions are also gratefully acknowledged.

References

1) E. Witten, Nucl. Phys. **B160** (1979) 57
2) R. Machleidt, K. Holinde and C. Elster, Phys. Reports **149** (1987) 1
3) R. Büttgen, K. Holinde, B. Holzenkamp and J. Speth, Nucl. Phys. **A450** (1986) 403;
B. Holzenkamp, K. Holinde and J. Speth, Nucl. Phys. **A500** (1989) 485
4) R. Büttgen, K. Holinde and J. Speth, Phys. Lett. **B163** (1985) 305;
R. Büttgen, K. Holinde, A. Müller-Groeling and P. Wyborny, Nucl. Phys., in press
5) G.E. Brown, J.W. Durso, M.B. Johnson and J. Speth, Phys. Lett. **B238** (1990) 20
6) W. Ferchländer and D. Schütte, Phys. Rev. **C22** (1980) 2536
7) G. Mennessier, Z. Phys. **C16** (1983) 241

8) J. Donoghue, C. Ramirez and G. Valencia, Phys. Rev. **D38** (1988) 2195
9) M.I. Haftel and F. Tabakin, Nucl. Phys. **A158** (1970) 1
10) M. Gell-Mann and Y. Ne'eman, The eightfold way (Benjamin, New York, 1964)
11) T. Fujiwara, T. Kugo, H. Terao, S. Uehara and K. Yamawaki, Prog. Theor. Phys. **73** (1985) 926
12) J. Gasser and H. Leutwyler, Ann. of Phys. **158** (1984) 142
13) M. Bando, T. Kugo, S. Uehara, K. Yamawaki and T. Yanagida, Phys. Rev. Lett. **54** (1985) 1215
14) R. Bhaduri, Models of the nucleon from quarks to solitons, (Addison-Wesley, Reading, MA 1989) Ch. 7
15) J.W. Durso, Phys. Lett. **B184** (1987) 348
16) T.D. Lee, Phys. Rev. **95** (1954) 1329
17) C.D. Frogatt and J.L. Petersen, Nucl. Phys. **B129** (1977) 89
18) S.D. Protopopescu *et al.*, Phys. Rev. **D7** (1973) 1279
19) B.R. Martin, D. Morgan and G. Shaw, "Pion-pion interactions in particle physics (Academic Press, London, 1976)
20) R. Jaffe, Phys. Rev. **D15** (1977) 267
21) J. Weinstein and N. Isgur, Phys. Rev. **D27** (1983) 588; preprint UTPT-89-03
22) T. Barnes, Phys. Lett. **B165** (1985) 434
23) W. Ochs, thesis, Universität München, 1973
24) M.N. Cason *et al.*, Phys. Rev. **D28** (1983) 1586
25) Particle Data Group, Phys. Lett. **B204** (1988)
26) A. Etkin *et al.*, Phys. Rev. **D25** (1982) 1786
27) A.B. Wicklund *et al.*, Phys. Rev. Lett. **45** (1980) 1469
28) D. Cohen *et al.*, Phys. Rev. **D22** (1980) 2595
29) A.D. Martin and E.N. Ozmutlu, Nucl. Phys. **B158** (1977) 520
30) O. Dumbrajs *et al.*, Nucl. Phys. **B216** (1983) 277
31) A. Firestone, G. Goldhaber, D. Lissanes and G.H. Trilling, Phys. Rev. **D5** (1972) 2188
32) P. Estabrooks *et al.*, Nucl. Phys. **B133** (1978) 496
33) M.J. Matison, *et al.*, Phys. Rev. **D9** (1974) 1872
34) D. Aston *et al.*, Nucl. Phys. **B296** (1988) 293
35) C.B. Lang, Fort. der Phys. **26** (1978) 509
36) B. Jongejans *et al.*, Nucl. Phys. **B67** (1973) 381